Pulse Wave Propagation in the Arterial Tree

Frans N. van de Vosse[1] and Nikos Stergiopulos[2]

[1]Department of Biomedical Engineering, Eindhoven University of Technology, 5600 MB Eindhoven, The Netherlands; email: F.N.v.d.Vosse@tue.nl

[2]Laboratory of Hemodynamics and Cardiovascular Technology, Swiss Federal Institute of Technology, 1015 Lausanne, Switzerland; email: nikolaos.stergiopulos@epfl.ch

Annu. Rev. Fluid Mech. 2011. 43:467–99

First published online as a Review in Advance on September 22, 2010

The *Annual Review of Fluid Mechanics* is online at fluid.annualreviews.org

This article's doi: 10.1146/annurev-fluid-122109-160730

0066-4189/11/0115-0467$20.00

Keywords

hemodynamics, arterial mechanics, blood flow, blood pressure, pulse wave velocity, wave reflections, 1D modeling

Abstract

The beating heart creates blood pressure and flow pulsations that propagate as waves through the arterial tree that are reflected at transitions in arterial geometry and elasticity. Waves carry information about the matter in which they propagate. Therefore, modeling of arterial wave propagation extends our knowledge about the functioning of the cardiovascular system and provides a means to diagnose disorders and predict the outcome of medical interventions. In this review we focus on the physical and mathematical modeling of pulse wave propagation, based on general fluid dynamical principles. In addition we present potential applications in cardiovascular research and clinical practice. Models of short- and long-term adaptation of the arterial system and methods that deal with uncertainties in personalized model parameters and boundary conditions are briefly discussed, as they are believed to be major topics for further study and will boost the significance of arterial pulse wave modeling even more.

1. INTRODUCTION

1.1. Background

The functioning of the cardiovascular system has been a subject of scientific research since ancient times. Many researchers have dedicated significant parts of their scientific lives to the investigation and modeling of the cardiovascular system, including not only physicians, looking for the causes and treatments of cardiovascular disease, but also many physicists, mathematicians, and engineers, intrigued by the function of the cardiovascular system. Due to progress in computational methods and resources, and advances in our knowledge of cardiovascular physiology, models of arterial blood flow have evolved in the course of years from relatively simple one-dimensional (1D) models, based on mass and momentum conservation integrated over the cross-sectional area of the arteries such as in Anliker et al. (1971) or 0D lumped transition line network versions such as in Westerhof et al. (1969), to more complex 3D models based on approximate numerical solutions of the full set of equations of motion for fluid-structure interaction (see, e.g., Taylor & Figueroa 2009, van de Vosse et al. 2003). In recent years, however, there has been a revival of the simpler 1D models because of their power to supply boundary conditions for more complex 3D fluid-structure interaction models, used to better understand and analyze local biological and physiological processes in the arterial system, and because of the relative ease of their application to a more global patient-specific context, used to advance diagnostics and medical treatment in the clinic. A key issue in these 1D models is pulse wave propagation in the arterial tree: the title and subject of this review.

1.2. Aim and Outline

Rather than giving a general survey of the literature on pulse wave propagation in the arterial tree, this review gives an overview of the most important aspects concerning the physical understanding and possible application of this phenomenon. Accordingly, the present review starts with a short introduction to cardiovascular physiology and pathology as seen through the eyes of a fluid dynamicist, followed by a brief historical outline of pulse wave-propagation studies and their applications. This review then focuses on the physical and mathematical background, starting from the description of pressure and flow waves in straight vessels, forming the basis of pulse wave phenomena in the arterial tree. Attention is paid to wave reflection and transition at geometrical or constitutive discontinuities such as arterial bifurcations and sudden changes of vessel-wall mechanical properties. Next, general remarks on possible and admissible inflow and outflow conditions and the way in which they can be applied are provided. Lumped models for the heart and the microcirculation are briefly introduced, and a short discussion on how the venous tree can close the system is given. The next section is dedicated to experimental work that has been performed both in vivo and in vitro, to validate mathematical and computational models, as well as to evaluate the applicability of the models to physiologically and clinically relevant settings. Finally, future directions concerning short- and long-term adaptation and patient-specific modeling are given and final conclusions are made.

2. PHYSIOLOGICAL AND HISTORICAL SETTING

2.1. Cardiovascular Physiology

The cardiovascular system (see **Figure 1**) provides convective transport of blood (and its contained gases, cells, particles, and heat) between the different organs of the body. Due to the high resistance against flow in the microcirculation, the transport of blood requires a relatively high perfusion

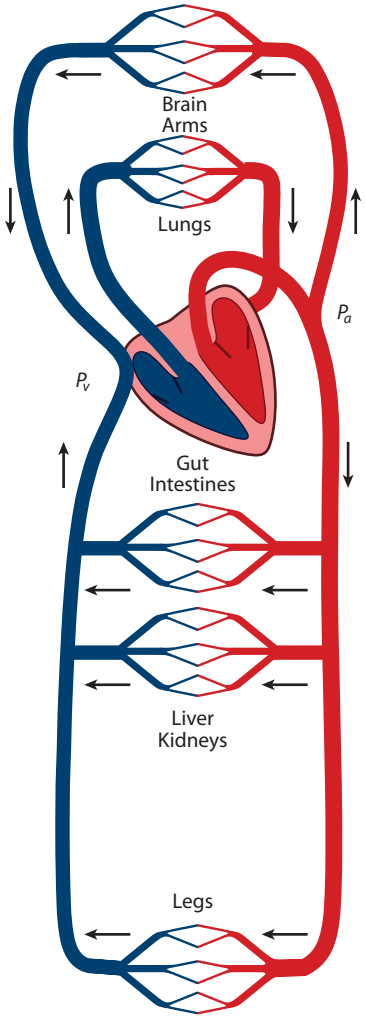

Figure 1

Overview of the cardiovascular system, showing the heart as a pump, the pulmonary and systemic circulation in series, a bifurcating network of arteries, the microcirculation in the tissues, and the venous system.

pressure. Maintenance of high levels of perfusion pressure without overloading the pumping heart is only possible when the arterial network is elastic (the windkessel effect). An extended overview of physiological processes needed by, and enabled through, the cardiovascular system can be found in standard textbooks on physiology such as Guyton (1967) and Boron & Boulpaep (2003).

2.1.1. The heart. The forces needed for the motion of the blood are provided by the heart, which serves as a four-chambered pump that propels blood through the circulatory system (see **Figure 2**). A complete heart cycle consists of a number of phases, more or less similar for the right and left parts. For the left part, the onset of these phases is indicated in **Figure 3**, where the left ventricular pressure, aortic pressure, and aortic flow are given as a function of time

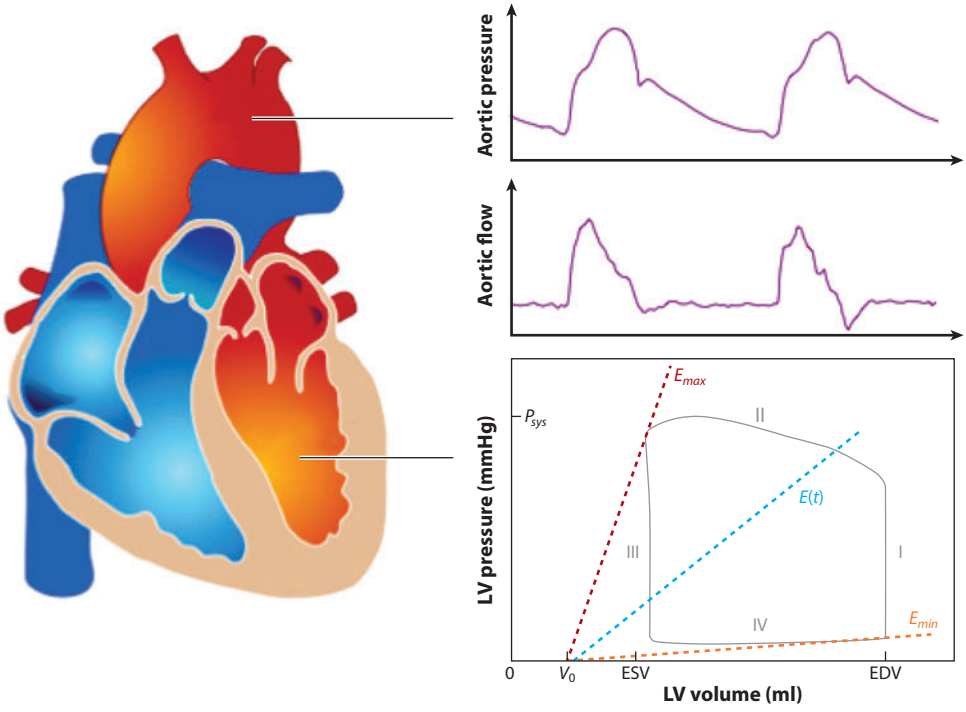

Figure 2

A schematic of the heart together with aortic pressure and flow curves and the left ventricular (LV) pressure-volume loop. ESV and EDV denote the end systolic and end diastolic volume, respectively.

during a cardiac cycle. Because both the blood flow velocities and the geometrical length scales are relatively large, $U = O(1\ \mathrm{m\ s^{-1}})$, $L = O(0.01\ \mathrm{m})$, in the heart, its fluid mechanics is strongly determined by inertial forces that are in equilibrium with pressure forces, $Re = U\,L/\nu > O(2{,}500)$, $Sr = fL/U = O(0.1)$.

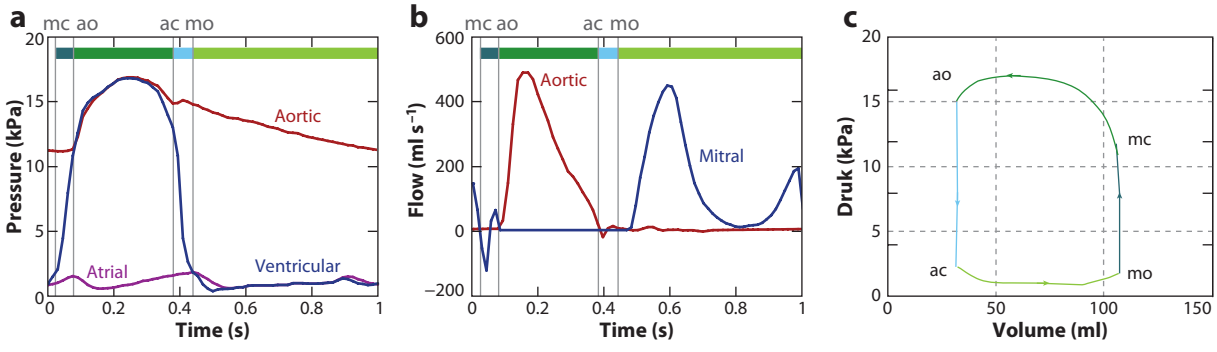

Figure 3

(*a*) Aortic, ventricular, and atrial pressure; (*b*) aortic and mitral flow; and (*c*) left ventricular pressure-volume curves. The time periods between closure of the mitral valve (mc), opening of the aortic valve (ao), closure of the aortic valve (ac), and opening of the mitral valve (mo) are indicated.

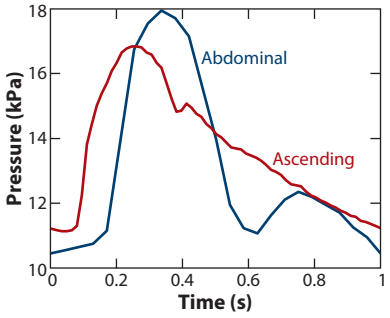

Figure 4

Pressure in the ascending and abdominal aorta ≈0.5 m apart from each other, showing a time difference of $O(0.1\ \text{s})$ between the feet of both pulses and thus a wave speed of approximately 5 m s^{-1}.

2.1.2. The arterial tree. The arterial system is responsible for the transport of blood to the tissues. The pressure is kept at a relatively high value because the distal end of the arterial system bifurcates into many vessels with small diameters (arterioles) and hereby forms a large peripheral resistance. Pressure pulsations are reduced by the elasticity of the vessels (the windkessel effect). This elastic function of the arteries also aids perfusion during diastole and produces the wave-propagation phenomenon, which is the subject of this review. Smooth muscle cells in the arterial wall can change their contractile state, thereby changing the diameter and hemodynamical resistance. In this way blood flow is distributed to the different vascular beds in accordance with the local instantaneous metabolic needs. In the arterial system, unlike the situation in the heart, viscous forces may become significant, $Re < O(500)$, $Sr = O(0.05)$, as a result of a decrease in characteristic velocity and length scales.

Pressure in the aorta changes significantly with increasing distance from the heart. There is a phase shift in the pressure pulse, indicating wave propagation along the aorta with a specific wave speed. The shape of the pressure pulse changes and shows an increase in amplitude, a steepening of the front, and a moderate fall of the mean pressure (see **Figure 4**). This wave phenomenon is a direct consequence of the distensibility of the arterial wall. The instantaneous cross-sectional area of the vessels depends on the transmural pressure difference across the wall denoted by p_{tr}. Due to the complex nonlinear anisotropic and viscoelastic properties of the arterial wall, the relation between the transmural pressure and the cross-sectional area A of the vessel is nonlinear and frequency dependent. Important quantities with respect to this relation, used in physiology, are the compliance C of the vessel, which depends on p_{tr} and is defined as

$$C(p_{tr}) = \frac{\partial A}{\partial p_{tr}}. \tag{1}$$

A typical example of experimental data is given in **Figure 5**. As depicted, compliance depends strongly on pressure. At high transmural pressures, the artery becomes stiffer, due to the progressive recruitment of stiff collagen fibers in bearing the load.

2.1.3. The microcirculation. In the microcirculation, the blood flows through the arterioles into the capillary system, a network of small vessels with walls consisting of a single layer of endothelial cells lying on a basement membrane. Here, an exchange of blood gases and nutrients with the interstitial liquid in the tissues takes place. The diameter of the capillaries is small enough that the whole blood may not be considered as a homogeneous fluid anymore. The blood cells move in a single-file train and deform strongly. The plasma, together with the glycocalyx layer

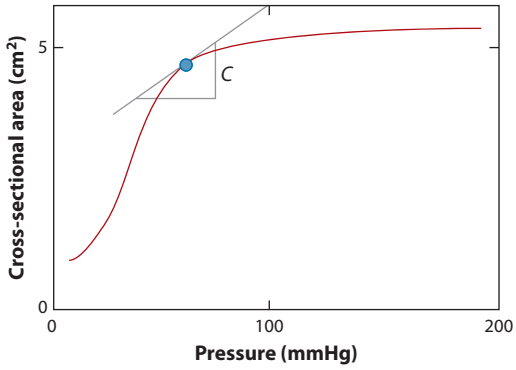

Figure 5

Typical area-pressure relation for a human thoracic aorta showing a nonlinear behavior. Compliance is defined as the slope of the area-pressure curve and is strongly dependent on pressure.

covering the endothelial cells, acts as a lubrication layer (Damiano 1998). In the microcirculation, viscous forces dominate over inertia forces, $Re < O(1)$. Consequently, in its most simple form, the microcirculation, including the arterioles, can be approximated as a collection of parallel tubes or a porous media with a linear relation between perfusion pressure and flow, given by

$$p_a - p_v = qR_p, \tag{2}$$

with the perfusion pressure defined as the difference between the arterial pressure p_a and the venous pressure p_v. In general, the peripheral resistance R_p is not a constant and is principally controlled by the smooth muscle tone of the arterioles.

2.1.4. The venous system. The blood is collected in the venous system (venules and veins) in which the vessels rapidly merge into larger vessels directing the blood back to the heart. As the diameters in the venous system are of the same order of magnitude as in the arterial system, inertia forces may become influential again. However, both characteristic velocities and pressure amplitudes are lower than in the arterial system. As a consequence, in the venous system, unsteady inertia forces are of less importance than in the arterial system. Also the pressure within the veins is significantly lower than the arterial pressure: $O(1\text{ kPa})$ versus $O(10\text{ kPa})$. In certain situations the pressure can be low enough that the normal functioning vein will have an elliptic cross-sectional area or even collapse. Because of low pressures, gravitational forces become important, especially in the upright position. To cope with gravitational effects, veins dispose valves to prevent retrograde flow and insure unidirectional flow toward the heart.

2.2. Cardiovascular Pathology

Heart failure and arteriosclerosis are general terms for several diseases that compose the majority of disorders that may affect the cardiovascular system. In this section a few words are spent to indicate how blood pressure and blood flow are key players in the development and course of these diseases.

2.2.1. Heart failure. Heart failure refers to a cardiac dysfunction in which the heart may not pump enough blood. In systolic dysfunction, the myocardial contraction is diminished, and as a result, blood accumulates in the lungs or veins. Coronary artery disease, leading to a reduction

of the flow of oxygen-rich blood to the heart muscle, is a common cause of systolic dysfunction. Also heart-valve disorders such as stenosis or leakage can cause systolic dysfunction as, over time, due to inadequate emptying of the ventricles, the heart enlarges and cannot pump adequately anymore. In diastolic dysfunction, the heart muscle has become stiffer and does not relax normally after contracting, which makes filling with blood less effective. High blood pressure is the most common cause of diastolic dysfunction. This is because the heart must eject blood against the higher pressure in the arterial system, causing the heart's walls to thicken (hypertrophy) and stiffen.

2.2.2. Vascular disorders. Vascular disorders are primarily related to arteriosclerosis. Arteriosclerosis means hardening (sclerosis) of the arteries (arterio-) and usually affects all humans as part of the aging process. Atherosclerosis, in which fatty deposits (plaques) develop in the walls of medium-sized and large arteries, is the most common type of arteriosclerosis causing symptoms. Various factors, including high blood pressure, diabetes, and high levels of cholesterol in the blood, may contribute to this development. Hemodynamical factors such as disturbed blood flow, low wall shear rate, and wall shear stress favor the development of atherosclerosis. This is why regions of disturbed blood flow, such as bifurcations and curved vessels, appear to be more prone to atherosclerosis. Plaques can grow and gradually cause the artery to narrow, compromising blood flow. Plaques can also rupture, exposing the lipid material within to the bloodstream. This can trigger the formation of a blood clot, which can suddenly block all blood flow or detach and travel downstream, creating an embolism. Heart attacks due to coronary artery disease and stroke (resulting from atherosclerosis that affects the arteries to the brain) are responsible for more deaths than all other causes combined.

Atherosclerotic processes are also seen as the most common cause of aortic aneurysms. Atherosclerosis locally weakens the vascular wall. The transmural arterial pressure forces the weak area to remodel and bulge outward. An aortic aneurysm may rupture, resulting in an often fatal internal bleeding. High blood pressure, which is common among older people, increases the risk of aneurysm development. Aneurysms may also occur in the arteries of the brain (cerebral arteries). Rupture of a cerebral aneurysm may cause bleeding into the brain tissue, resulting in a hemorrhagic stroke.

2.3. Importance of Arterial Pressure and Flow Modeling

From the above sections, the importance of arterial pressure and the associated flow phenomena in the development of cardiovascular disorders is evident. It is also clear that for vascular diseases, local blood flow characteristics play a determinant role in the development and progression of disease and thus should be studied in detail. However, there are physiological situations and pathologies of major clinical interest for which local details in flow are not important. What is important for these cases is the distribution of pressure and flow waves in the arterial tree. A famous example is isolated systolic (or old-age) hypertension, which results from the interaction between the pumping heart and the arterial system (load) and in which augmented pressure wave reflections due to arterial stiffening with age are thought to be important determinants. It is therefore important to understand and to be able to analyze pressure and flow wave phenomena in the arterial tree. Knowledge of pressure and flow distributions in the arterial tree is also indispensable in diagnostics and planning of treatment. Modeling of the cardiovascular system is one way to acquire this knowledge.

Modeling arterial blood flow is challenging, due to obvious difficulties in describing the geometry of the arterial tree, the nonlinear wall viscoelasticity, and non-Newtonian rheological

properties of blood. Also challenging is the description of proximal and distal boundary conditions. The inflow into the aorta is given by the complex interaction between the pumping heart and the arterial load (afterload), whereas the outflow into the venous circulation necessitates the description of the microcirculation, a formidable task to perform in full detail. Thus, researchers have resorted to the use of models, which contain a manageable number of parameters and allow for an accurate modeling of arterial blood flow. Models of arterial blood flow may be classified into three major categories.

2.3.1. Windkessel or 0D models. Windkessel models provide for an overall lumped description of the arterial tree but do not permit studies on pressure and flow wave propagation therein. They give the relation between pressure and flow at a specific arterial site. Their main advantage is that they contain only a few parameters representing the main properties of the arterial tree distal to the point of interest.

2.3.2. Distributed or 1D models. Distributed models are formed by breaking up the arterial tree into small segments whose geometry and mechanical properties are known. The wave-transmission characteristics of each arterial segment can be described using Womersley's (1957) oscillatory flow theory or electrical transmission line theory. Distributed models of the arterial tree can also be constructed based on the 1D form of the Navier-Stokes equations for the conservation of mass and momentum, as described in Section 3.3.

2.3.3. 3D models. These models are usually applied when a detailed description of the 3D flow field is needed, usually at a specific part of the arterial tree where fluid phenomena are complex and of physiological or pathological interest (e.g., near a bifurcation, within an aneurysm, or in the vicinity of a heart valve or a stenosis). 3D models can yield characteristics that 1D models cannot, such as the wall shear stress field or the vorticity field, but are computationally much more intense and are sensitive to boundary conditions, which are often not known in detail. 3D models involve computational fluid dynamics (CFD) approaches, the most recent of which have been extended to include fluid-structure interactions between blood and the arterial wall (see also Heil & Hazel 2011). The computational intensity of fluid-structure interaction models is such that the models are generally applied only to restricted local areas and not to the study of wave-propagation phenomena in the entire arterial tree or major parts of it.

The choice of model depends on the degree of detail in arterial blood flow required. To understand the effect of global arterial parameters (i.e., total arterial resistance or total arterial compliance) on integrated quantities such as aortic pressure and cardiac output, windkessel models suffice. To model local flows and pressures and their transmission, one needs to use distributed or 1D models, whereas local flow-field details can only be obtained from 3D models. Depending on the objective, combinations of models or multiscale models can be employed. For example, 1D models of the entire arterial tree, terminated with 0D models at the distal ends (see **Figure 6**), have been used to provide realistic local boundary conditions for 3D CFD simulations at the specific arterial site (Beulen et al. 2009, Quarteroni & Veneziani 2003, Taylor & Figueroa 2009).

2.4. Historical Overview

The arterial pulse was known as a vital sign to the ancient Greeks, Romans, Indians, and Chinese, who exploited its diagnostic value for thousands of years. The notion of wave propagation was not known to them. The concept of circulation also remained unknown until the seminal work of

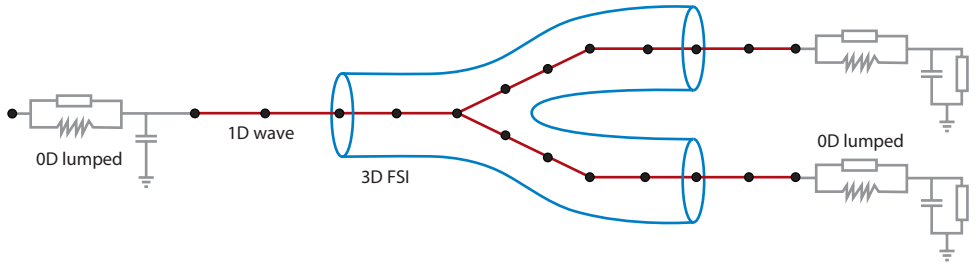

Figure 6

Coupling of 3D, 1D, and 0D models to perform a fluid-structure interaction (FSI) analysis of the flow and wall motion in an arterial bifurcation.

Harvey (1957 [1628]), who lived in the period 1578–1657 (see Parker 2009a for an overview). It was Leonhard Euler who wrote the first set of 1D equations, based on conservation of mass and momentum, for studying wave propagation in arteries. Euler failed to solve his set of 1D equations due to unrealistic wall constitutive laws. The relation of wave speed to blood properties and wall elasticity was first given by Young (1809), expressed as

$$c = \sqrt{\frac{A}{\rho C}}, \tag{3}$$

where c is wave speed, and C is local area compliance (see Equation 1). Later in the nineteenth century, Moens published an experimental work on wave speed in arteries and Korteweg published a theoretical study on wave speed in elastic tubes, which for thin-walled arteries is expressed by the well-known Moens-Korteweg relation:

$$c = \sqrt{\frac{Eh}{2\rho a}}, \tag{4}$$

where E is the elastic modulus of the wall, h the wall thickness, and $2a$ the luminal diameter. Direct estimation of wave speed at a given arterial location requires the knowledge of local dimensions and local elastic properties. There are other alternative indirect methods for assessing wave speed. The most popular is to measure the travel time Δt of the foot of the pressure wave over a distance Δx, so that the average wave speed in the arterial segment is $c = \Delta x/\Delta t$. For a more detailed discussion on the different methods for estimating wave speed, the reader is referred to Westerhof et al. (2005) and Davies et al. (2006).

2.4.1. Lumped parameter models. The first lumped parameter model of the arterial system was the two-element windkessel model by Frank (1899). Based on an analogy to electrical circuits, the two-element windkessel model considers the entire arterial tree as a parallel combination of total arterial compliance C and peripheral resistance R. The model predicts an exponential decay of pressure in the aorta during diastole when the aortic valve is closed and flow is zero. Frank originally developed the two-element windkessel to obtain cardiac-output estimates from pressure measurements in the aorta. The decay time constant is given by the product of peripheral resistance and total arterial compliance $\tau = RC$. Hence by determining the diastolic decay time and knowing the peripheral resistance, one can easily obtain estimates of total arterial compliance. In the frequency domain, the two-element windkessel yields an input impedance modulus, which represents the true input impedance at the aorta well, but drops asymptotically to zero at high frequencies. In reality, input impedance at high frequencies equals the characteristic impedance of

the aorta: $Z_c = \rho c / A$. To address this shortcoming, the three-element windkessel model was proposed by Westerhof et al. (1971), in which a resistance equal to Z_c is located upstream and in series with the two-element windkessel model. However, the approximation of characteristic impedance by a resistor leads to errors in the low-frequency range. The fourth element of the windkessel was introduced to circumvent the inconsistency resulting from modeling the characteristic impedance by a resistance (Stergiopulos et al. 1999). The fourth element of the windkessel is the total arterial inertance, placed parallel with the characteristic impedance. This way the four-element windkessel model becomes asymptotically equal to the two-element model at low frequencies and equal to the three-element model at high frequencies, yielding a better approximation of the true aortic input impedance (Stergiopulos et al. 1999).

2.4.2. Pulsatile tube flow theory. The solution for pulsatile flow in rigid tubes was first given by Witzig (1914). Womersley (1955) gave the solution for the velocity profile in a rigid tube driven by a harmonic pressure gradient with amplitude $\widehat{\frac{\partial p}{\partial z}}$ and circular frequency ω as

$$v(r,t) = Re\left[\frac{i}{\rho\omega}\widehat{\frac{\partial p}{\partial z}}\left\{1 - \frac{J_0(i^{3/2}\alpha y)}{J_0(i^{3/2}\alpha)}\right\}e^{i\omega t}\right], \tag{5}$$

where y is the relative radial position, $y = r/a$, and $i = \sqrt{-1}$. Flow is given as

$$q(t) = Re\left[i\frac{\pi a^2}{\rho\omega}\widehat{\frac{\partial p}{\partial z}}\{1 - F_{10}(\alpha)\}e^{i\omega t}\right], \tag{6}$$

with $F_{10}(\alpha)$ the Womersley function given by

$$F_{10}(\alpha) = \frac{2J_1(i^{3/2}\alpha)}{i^{3/2}\alpha J_0(i^{3/2}\alpha)}, \tag{7}$$

where $\alpha = a\sqrt{\omega\rho/\eta}$ is the Womersley parameter, and J_0 and J_1 are Bessel functions of order 0 and 1, respectively. Womersley (1955, 1957) went on to provide solutions for pulsatile flow in tubes with elastic walls and to include wall viscoelasticity and longitudinal constraints. Important early work in the time domain was published by Ling & Atabek (1972). Unlike Womersley's theory, which is formulated in the frequency domain, and allows for analytical solutions, time-domain formulations can only result in approximate solutions obtained by numerical integration.

2.4.3. Distributed and 1D models. The windkessel models give a global lumped description of the arterial tree distal to a specific arterial site. If this site is the proximal aorta, then the windkessel model will give a lumped representation of the entire arterial tree. Windkessel models do not account for pressure and flow wave propagation in the arterial tree. Modeling wave propagation requires the use of tube models or distributed models that account for arterial geometry and wall elasticity. The basic idea of distributed models is to break up the arterial tree into small segments whose geometry and mechanical properties are known. The wave-transmission characteristics of each arterial segment can be described using Womersley's (1957) oscillatory flow theory or electrical transmission line theory (Westerhof et al. 1969). Alternatively, distributed models of the arterial tree can be constructed based on the 1D (simplified) form of the blood flow equations describing the conservation of mass and momentum, such as Equation 19 developed in Section 3.2.

The continuity and momentum equations have three variables: pressure p, flow q, and area A. Therefore, a constitutive law relating cross-sectional area, A, to pressure, p, is needed to form a system of three equations with three unknowns, which can be easily solved using different numerical techniques (i.e., finite differences or method of characteristics). Distributed models have

been extensively used, for example, to study different aspects of pressure and flow propagation, the effects of different forms of arterial disease on pressure and flow waves, wave reflections, and the relation of peripheral to central pressure waves. The accurate predictions of pressure and flow combined with their ease of use and low computational intensity make 1D models of the circulation useful research tools.

3. PHYSICAL AND MATHEMATICAL BACKGROUND

3.1. Basic Equations

In this section the mass and momentum balance equations that form the basis for the 1D wave propagation models are derived from a 1D form of the Reynolds transport theorem.

3.1.1. The 1D Reynolds transport theorem. Following the work of Hughes & Lubliner (1973), we take the geometry depicted in **Figure 7** as a point of departure. The volume V is bounded by proximal and distal planes A_p and A_d perpendicular to the z axis at fixed locations z_p and z_d, respectively. The lateral surface of V is denoted by S_l and is allowed to move with velocity $\boldsymbol{u}$. The outward normal to the surfaces A_p, A_d, and S_l is denoted by $\boldsymbol{n}$. For this configuration, the Reynolds (1903) transport theorem can be written as

$$\frac{d}{dt}\int_{V(t)} \psi\, dV = \int_{V(t)} \frac{\partial \psi}{\partial t} dV + \int_{S(t)} \psi \boldsymbol{u}\cdot\boldsymbol{n}\, dS. \tag{8}$$

Here $\psi = \psi(\boldsymbol{x}, t)$ is an arbitrary function; dV and dS are infinitesimal volume and surface elements, respectively; and $S = S_l + A_p + A_d$ is the surface that closes volume V. We let $\bar{\psi}$ be the average value of ψ on the luminal area:

$$\bar{\psi}(z,t) = \frac{1}{A}\int_{A(z,t)} \psi\, dA. \tag{9}$$

Knowing that z_p and z_d are fixed and independent of time, we find for the 1D Reynolds transport equation

$$\frac{\partial}{\partial t}(A\bar{\psi}) + \frac{\partial}{\partial z}(A\overline{\psi v_z}) = \int_{A(z,t)} \dot{\psi}\, dA + \oint_{l(z,t)} \psi w_n dl, \tag{10}$$

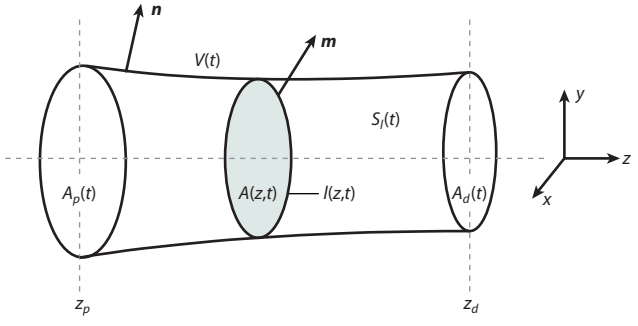

Figure 7

The geometry of a part of a vessel along the z axis, bounded by the cross-sectional surfaces A_p at $z = z_p$ and A_d at $z = z_d$. The total volume is denoted by the symbol V. An arbitrary cross section perpendicular to the axis is denoted by A and its boundary by l.

with $w_n = \boldsymbol{w} \cdot \boldsymbol{n}$ the normal component of $\boldsymbol{w} = \boldsymbol{u} - \boldsymbol{v}$ on curve l (see also Hughes & Lubliner 1973). This is the basis to derive the equations for conservation of mass and momentum given in the next section.

3.1.2. The 1D mass balance. If we take $\psi = 1$ in the local Reynolds transport equation (Equation 10), we obtain the integrated continuity equation in area-velocity (A, v) formulation, localized with respect to the axial coordinate z:

$$\frac{\partial A}{\partial t} + \frac{\partial}{\partial z}(Av) + \Psi = 0. \tag{11}$$

Here $v = \overline{v_z}$ denotes the cross-sectional mean of the velocity in the z direction, and the volumetric outflow per unit length Ψ is given by

$$\Psi = -\oint_l w_n dl. \tag{12}$$

So far we have followed the derivations given in Hughes & Lubliner (1973). Introduction of the volume flow $q \equiv Av$ gives the equivalent area-flow (A, q) formulation as, e.g., used by Wan et al. (2002):

$$\frac{\partial A}{\partial t} + \frac{\partial q}{\partial z} + \Psi = 0. \tag{13}$$

Substitution of the constitutive relation, expressing the response of the vessel wall to transmural pressure variations, according to Equation 1 with $p_{tr} = p$ results in an equivalent pressure-flow (p, q) formulation:

$$C\frac{\partial p}{\partial t} + \frac{\partial q}{\partial z} + \Psi = 0. \tag{14}$$

Here $C(z, t)$ is the compliance of the vessel that can be obtained either from experimental data or from a solid mechanics model of the arterial wall.

3.1.3. The 1D momentum balance. The momentum balance equation for the fluid inside the vessel in three dimensions is

$$\rho \dot{\boldsymbol{v}} = \rho \boldsymbol{f} + \nabla \cdot \boldsymbol{\sigma}, \tag{15}$$

with ρ the density of the fluid, $\boldsymbol{v}$ the velocity, $\boldsymbol{f}$ the body forces, and $\boldsymbol{\sigma}$ the Cauchy stress tensor, which, for (generalized) Newtonian fluids, is given by $\boldsymbol{\sigma} = -p\boldsymbol{I} + 2\eta\boldsymbol{D}$, with η the viscosity and $\boldsymbol{D}$ the rate of deformation tensor. We let the characteristic axial length scale L_z be defined as the minimum of the wavelength λ of pressure and flow waves traveling through the arteries and the wavelength or curvature associated with axial changes in the cross-sectional area $(\partial A/\partial z)$. The following scaling is introduced for the coordinates $(x', y') = (x, y)/a_0$, $z' = z/L_z$, with $a_0 = \sqrt{A_0/\pi}$. The velocity can be scaled according to $(v'_x, v'_y) = (v_x, v_y)/U$, $v'_z = v_z/V$ with $U = (a/L_z)V$. Under the assumption that body forces are small [$f_z \ll U^2/L_z$ and $\max(f_x, f_y) \ll V^2/a$] or work mainly in the axial direction [$f_z \gg (L_z/a_0)^2 \max(f_x, f_y)$], and in the case of long waves and gradual changes of the cross-sectional area ($L_z/a_0 \gg 1$), we can neglect all terms that scale with a_0/L_z. The pressure p is then constant over the cross-sectional area and only depends on z and t. The momentum balance equations will reduce to

$$\rho \dot{v}_z + \frac{\partial p}{\partial z} = \rho f_z + \nabla_A \cdot \boldsymbol{\tau}_A, \tag{16}$$

with Lagrangian time derivative $\dot{v}_z = \frac{\partial v_z}{\partial t} + \boldsymbol{v} \cdot \nabla v_z$ and a cross-sectional in-plane version of the extra stress $\boldsymbol{\tau}_A = \eta(\nabla_A \boldsymbol{v}_A + (\nabla_A \boldsymbol{v}_A)^T)$, with in-plane velocity $\boldsymbol{v}_A = v_x \boldsymbol{e}_x + v_y \boldsymbol{e}_y$ and gradient operator $\nabla_A = \boldsymbol{e}_x \frac{\partial}{\partial x} + \boldsymbol{e}_y \frac{\partial}{\partial y}$.

Integration of Equation 16 over the cross-sectional area A gives, after division by ρ and application of the divergence theorem on the last term,

$$\int_A \dot{v}_z dA + \frac{A}{\rho}\frac{\partial p}{\partial z} = Af_z + \oint_l \frac{\eta}{\rho}\frac{\partial v_z}{\partial m} dl, \tag{17}$$

with $\frac{\partial v_z}{\partial m} = \nabla_A v_z \cdot \boldsymbol{m}$ and $\boldsymbol{m} = (m_x, m_y, 0)$ the outerward normal to l. The first term of Equation 17 can be rewritten with the aid of the local Reynolds transport equation (Equation 10) for $\psi = v_z$. This yields

$$\frac{\partial Av}{\partial t} + \frac{\partial A\overline{v_z^2}}{\partial z} + \frac{A}{\rho}\frac{\partial p}{\partial z} = Af_z + \oint_l \left(\frac{\eta}{\rho}\frac{\partial v_z}{\partial m} + v_z w_n\right) dl. \tag{18}$$

Equation 18 is the 1D balance of momentum equation, almost identically derived by Hughes & Lubliner (1973), who substituted the 1D mass conservation given in Equation 13 to arrive at an (A, v) formulation for long waves ($L_z \gg a_0$). Substitution of $Av = q$ gives an equivalent (A, q) formulation. Motivated by the findings of Patel & Fry (1966), longitudinal tethering of the tube is assumed, allowing one to take $v_z = 0$ at the wall, so the second term in the closed path integral along the boundary l of the cross-sectional area can be discarded.

3.2. 1D Wave-Propagation Models

Based on the 1D mass balance (Equation 14) and the 1D momentum balance (Equation 18) different wave propagation models can be derived, depending on the terms that are taken into account and on the approximations that are made to describe the stationary inertia and the viscous forces. In this section different choices that can be made are described.

3.2.1. Dimensionless groups. If we define the wall shear stress as $\tau_w = \eta(\partial v_z/\partial m)$ and make use of the two aforementioned assumptions, together with the mass conservation equation given in Equation 14, we finally obtain

$$\begin{cases} C\dfrac{\partial p}{\partial t} + \dfrac{\partial q}{\partial z} + \Psi = 0 \\ \dfrac{\partial q}{\partial t} + \dfrac{\partial A\overline{v_z^2}}{\partial z} + \dfrac{A}{\rho}\dfrac{\partial p}{\partial z} = Af_z + \displaystyle\oint_l \frac{\tau_w}{\rho} dl. \end{cases} \tag{19}$$

If we scale according to $v_z = Vv_z'$, $p = (\rho V c_0)p'$, $t = (1/\omega)t'$, $q = (A_0 V)q'$, $A = A_0 A'$, $z = (\lambda/2\pi)z'$, $\Psi = \omega A_0 (V/c_0)\Psi'$, $f_z = (\omega V/A_0)f_z'$, $\tau_w = (\eta V/a_0)\tau_w'$, and $l = 2\pi a_0 l'$, the scaled dimensionless form is

$$\begin{cases} \left(\dfrac{\rho C}{A_0}\right)\dfrac{1}{c_0^2}\dfrac{\partial p'}{\partial t'} + \dfrac{\partial q'}{\partial z'} + \Psi' = 0 \\ \dfrac{\partial q'}{\partial t'} + \left(\dfrac{V}{c_0}\right)\dfrac{\partial A'\overline{v_z'^2}}{\partial z'} + A'\dfrac{\partial p'}{\partial z'} = A' f_z' + \dfrac{2}{\alpha^2}\displaystyle\oint_{l'} \tau_w' dl, \end{cases} \tag{20}$$

with $c_0 = \lambda(\omega/2\pi)$ and $\alpha = a_0\sqrt{\omega/\nu}$. If we take the parameter c_0, with the dimension of a velocity, equal to $c_0 = \sqrt{A_0/\rho C}$, then two dimensionless groups appear: the velocity ratio V/c_0 and the Womersley parameter α. If we take $\alpha \gg 1$ and $V/c_0 \ll 1$ and also consider the case without body forces f_z and volumetric outflow Ψ, a linearized version of Equation 19 with $A' = 1$ gives

$$\frac{\partial^2 p}{\partial t^2} - \frac{A_0}{\rho C}\frac{\partial^2 p}{\partial z^2} = 0, \tag{21}$$

representing pressure waves $p(z,t) = p_f(z - c_0 t) + p_b(z + c_0 t)$ that travel with a wave speed $c_0 = \sqrt{A_0/\rho C}$. Consequently the parameter c_0 can be associated with the wave speed at high

frequencies ($\alpha \gg 1$) and relatively low mean velocity ($v/c_0 \ll 1$), the Moens-Korteweg wave speed. In the arterial system α can vary from 20 in the aorta to near 0 in the smallest arteries, so the wall shear stress term cannot always be neglected. The velocity wave speed ratio, which can be seen as a kind of a Mach number, is typically smaller than 1 in normal physiological conditions, and only in the larger arteries may a significant contribution of the nonlinear advection term be expected. During exercise, when blood flow increases substantially, wave speed and mean velocity can have the same order of magnitude, and the nonlinear term should be taken into account. To solve Equation 19 with respect to q and p (or q and A), without neglecting any terms, one has to make assumptions regarding the shape of the velocity profile v_z in terms of q (or v) and p (or A) to evaluate the expressions containing $A\overline{v_z^2}$ and τ_w. Possible choices for this are given in the next section.

3.2.2. Velocity profile functions. A recent overview of 1D or distributed 0D models can be found in Reymond et al. (2009). From this overview we learn that most studies use rather simplified approximations for the velocity profile. In all studies, circular cross-sectional areas and axisymmetry are assumed, so $v_z(x, y, z, t) = v_z(r, z, t)$. With respect to velocity profile approximations, three categories can be identified.

Assumed shape profiles $v_z(r, z, t) = \phi(r)v(z, t)$. Here the velocity profile is written as the product of a radius-dependent profile function, independent of time, and the mean velocity that depends on the longitudinal coordinate and time. The following choices can be found in the literature (see also **Figure 9** in which the velocity profiles are shown for a carotid flow pulse as depicted in **Figure 8**):

Flat	$\phi(r) = 1,$
Poiseuille	$\phi(r) = 2(1 - (r/a)^2),$
Power law	$\phi(r) = \dfrac{n+2}{n}(1 - (r/a)^n),$
Assumed Stokes layer	$\phi(r) = \begin{cases} \phi_0 & \text{for} \quad r \le a(1 - 1/\alpha) \\ \phi_0\alpha(1 - r/a) & \text{for} \quad a(1 - 1/\alpha) < r \le a. \end{cases}$

The flat and Poiseuille profiles are used in many studies; the power-law profile was introduced by Hughes & Lubliner (1973) and used by Wan et al. (2002). The assumed boundary-layer profile

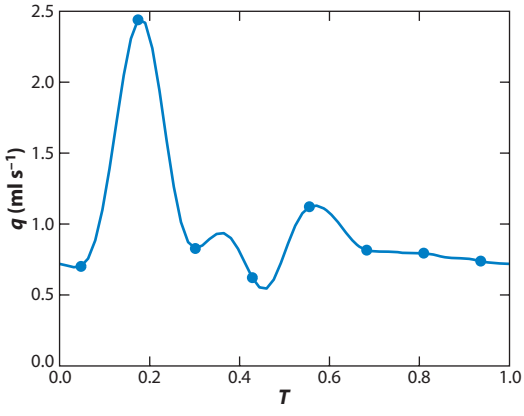

Figure 8

Typical carotid flow pulse used to construct the velocity profiles in **Figure 9**. Data taken from Holdsworth et al. (1999).

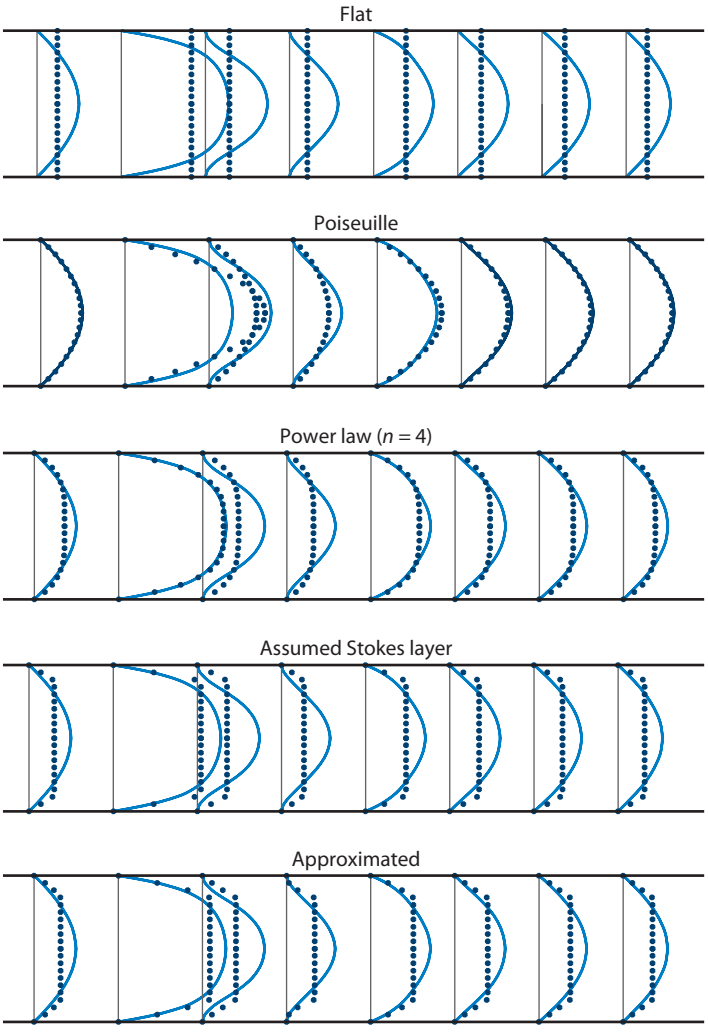

Figure 9

Different velocity profiles for the carotid flow pulse as depicted in **Figure 8**. The solid lines are the Womersley velocity profiles. The dotted lines represent the profiles as used in the different 1D models.

was introduced by Olufsen et al. (2000). The Stokes-layer thickness δ can be approximated by the viscous penetration depth based on the first harmonic, i.e., $\delta = \sqrt{\nu/\omega}$, with $\nu = \eta/\rho$ the kinematic viscosity. For the nonlinear and friction terms, this gives

$$A\overline{v_z^2} = \lambda(A)\frac{q^2}{A} \tag{22}$$

and

$$\tau_w = -\frac{a}{2}\gamma(\phi)Rq, \tag{23}$$

with a the radius, $\lambda(A)$ and $\gamma(\phi)$ dimensionless functions, and $R = \frac{8\eta}{\pi a^4}$ the Poiseuille resistance. A drawback in all these choices is that velocity profiles and corresponding wall shear stresses (see **Figure 10**) are in phase with flow, thus neglecting the inertia effects and the phase difference

Figure 10

Different approximations for the wall shear stress τ_w and nonlinear term $A\bar{v}_z^2$ for the typical carotid flow pulse given in **Figure 8**. $A_0 v_0^2$ is in units of 10^{-5} m^4 s^{-1}.

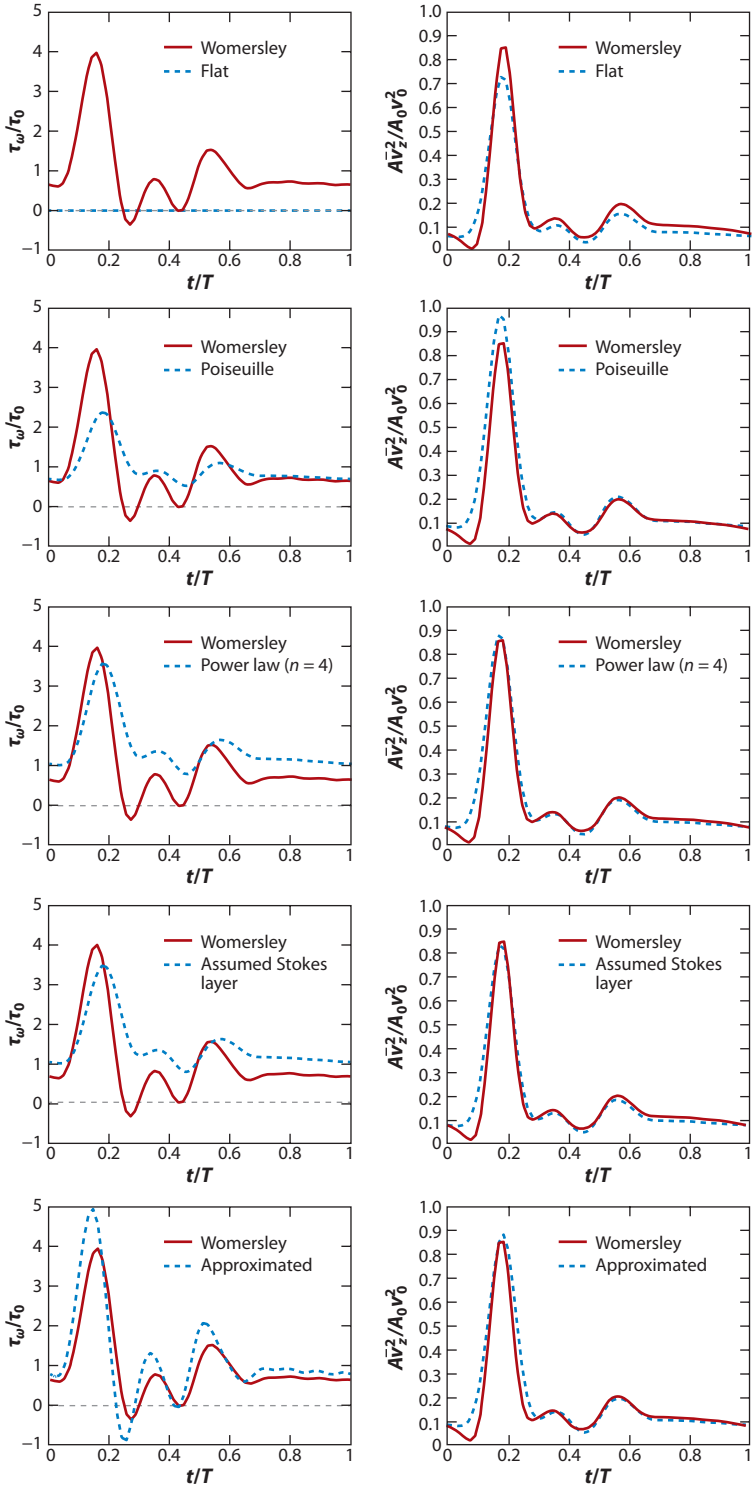

between flow q and the wall shear stress τ_w as predicted by Witzig-Womersley theory for 2D tube flow (Womersley 1957).

Time-periodic profiles $v_z(r, z, t) = \sum_n \phi(r)v_n(z)e^{i\omega_n t}$. To circumvent the above-mentioned disadvantage, Azer & Peskin (2007) and Reymond et al. (2009) employed the Womersley velocity profiles given in Equation 5 depending on the Womersley parameter $\alpha_n = a\sqrt{\omega_n/\nu}$ (see also **Figure 9**):

$$v_z(r, z, t) = \sum_{n=0}^{N} Re\left[\left\{1 - \frac{J_0(i^{3/2}\alpha_n r/a)}{J_0(i^{3/2}\alpha_n)}\right\}\frac{v_n(z)}{1 - F_{10}(\alpha_n)}e^{i\omega_n t}\right], \tag{24}$$

with the Womersley function as in Equation 7 and $v_n(z)$ the z-dependent n-th harmonic of the mean velocity.

This gives

$$A\overline{v_z^2} = \text{a nonalgebraic numerical integration}, \tag{25}$$

and according to Young & Tsai (1973b),

$$\tau_w = -\frac{a}{2}\left[c_v(\alpha)Rq + (c_u(\alpha) + 1)\frac{\partial q}{\partial t}\right], \tag{26}$$

with $c_v(\alpha)$ and $c_u(\alpha)$ dimensionless functions of α. For flows that are not time periodic, however, these profiles are not defined.

Approximated profiles $v_z(r, z, t) = \phi(r, z, t)v(z, t)$. Based on asymptotic solutions for the Stokes boundary layer and the central core of the tube, matched at the location of the Stokes boundary-layer thickness from the wall, Bessems et al. (2007) derived an approximate velocity profile expressed in p and q in the time domain, suitable for the approximation of $A\overline{v_z^2}$ and τ_w (see also **Figure 9**). In short this gives

$$Av_z^2 \approx \delta_1(\alpha)\frac{q^2}{A} \tag{27}$$

and

$$\tau_w = -\frac{a}{2}\left[c_q(\alpha)Rq - (c_p(\alpha) - 1)\frac{\partial p}{\partial z}\right]. \tag{28}$$

For high and low Womersley numbers, this approximation converges to the flat and Poiseuille approximation, and in between it agrees fairly well (see **Figure 10**) with solutions based on Womersley theory as derived by Young & Tsai (1973b).

In all cases given above, $\overline{v_z^2}(z, t) = \frac{2\pi}{A}\int_A v_z^2 r dr$ and $\tau_w(z, t) = -\eta\frac{\partial v_z}{\partial r}|_{r=a}$ can be expressed, either analytically or via numerical integration, in terms of the mean velocity $v(z, t)$.

3.3. Distributed 0D Models

If we take the general form of the 1D momentum equation from Equation 19 without nonlinear convection and body-force terms and a Poiseuille approximation for the friction term, a simple first-order finite-difference discretization in space results in a set of equations identical to the set of equations that can be derived from a three-element 0D module (see also **Figure 11*a***). Therefore, distributed 0D modeling can be seen as a spatial discretization of 1D wave-propagation models with first-order approximations of the spatial derivatives. As shown by Huberts et al. (2009b), such an analogy to electrical transmission line models can be made also for more complex 1D models, such as in the work of Bessems et al. (2007), with an approximate velocity profile. In this case, the

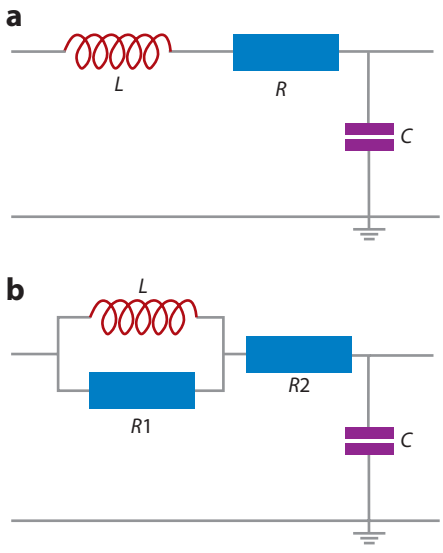

Figure 11

(*a*) A three-element and (*b*) a four-element 0D arterial segment. For possible definitions of *L*, *R*, *C*, *R*1, and *R*2, the reader is referred to Huberts et al. (2009b).

distributed model can be built from four-element 0D modules (see **Figure 11*b***) with parameters that depend on the Womersley number associated with the first harmonic.

We already showed that the 1D theory can make use of Womersley's (1957) 2D theory to obtain expressions for the velocity profile to be used to evaluate the nonlinear convection and friction term in Equation 19. In the frequency domain, the same theory can be used to define a characteristic impedance of an arterial segment relating the complex amplitudes of pressure and flow, i.e.,

$$Z_c = \frac{\hat{p}}{\hat{q}} = \frac{\rho c_0 / A_0}{\sqrt{1 - F_{10}(\alpha)}}, \tag{29}$$

with c_0 the Moens-Korteweg wave speed (see, e.g., McDonald 1974). Pressure and flow solutions then can be written as

$$p = Re\left[\hat{p}\, e^{i(\omega t - kz)}\right], \quad q = Re\left[\hat{q}\, e^{i(\omega t - kz)}\right], \tag{30}$$

with k the complex wave number given by

$$k = \frac{\omega}{c_0} \frac{1}{\sqrt{1 - F_{10}(\alpha)}}. \tag{31}$$

From the above equations, a longitudinal impedance Z_l can be derived according to

$$Z_l = -\frac{\hat{\partial} p}{\partial z} / \hat{q} = ikZ_c. \tag{32}$$

Two strategies can be followed to come to a distributed model. The first strategy is to use the general wave solution given in Equation 30 and expressions for the reflection coefficient at the transition to a subsequent arterial segment (see Section 3.4) to construct a transfer function between the pressures at the entrance and outflow of each segment (Avolio 1980). A second strategy (Huberts et al. 2009b) is to define an RLC network with Womersley number–dependent parameters based on Equation 32.

3.4. Wave Reflections

At transitions in geometrical or material properties (i.e., transitions in impedance) an incoming wave will partly be transmitted and partly be reflected. As a consequence, in the cardiovascular system all waves can be seen as a superposition of a forward and a backward traveling wave.

3.4.1. Forward and backward traveling waves. If the wave $p(z - ct)$ traveling in the forward direction is a solution of the wave equation given in Equation 21, then the wave $p(z+ct)$ traveling in the opposite direction is also a solution (i.e., the solutions p_f and p_b are constant along the characteristics $\Gamma : z = \pm ct$). For nonlinear waves satisfying Equation 19, two solutions will also be found based on the Riemann invariants that are constant along the characteristics, now being curved trajectories in the space-time plane (see, e.g., Lighthill 1978). Accordingly, at any location in the arterial tree, pressure and flow waves are the sum of waves traveling from the heart toward the periphery (forward running waves) and waves traveling from peripheral arteries toward the heart (backward running or reflected waves). Reflected waves arise from reflections of the forward running waves at arterial reflection sites, such as at bifurcations, stenoses, aneurysms, and all peripheral beds. The forward and backward running pressure and flow waves are related through the local characteristic impedance of the vessel: $\hat{p}_f = Z_c \hat{q}_f$ and $\hat{p}_b = -Z_c \hat{q}_b$. The measured pressure and flow are the sum of their forward and backward running components, so that we may write

$$p = p_f + p_b \quad \text{and} \quad q = q_f + q_b, \tag{33}$$

or equivalently (Westerhof et al. 1972)

$$\hat{p}_f = (\hat{p} + Z_c \hat{q})/2 \quad \text{and} \quad \hat{p}_b = (\hat{p} - Z_c \hat{q})/2. \tag{34}$$

If nonlinear effects arising from convective acceleration and nonlinear wall elasticity are included, wave separation needs to be done in the time domain. Such a nonlinear wave separation technique, based on the Riemann invariants, was developed by Pythoud et al. (1996). The analysis of arterial waves into their forward and backward running components can be used to assess the role of wave reflections in physiological and pathological situations. **Figure 12** shows aortic pressure

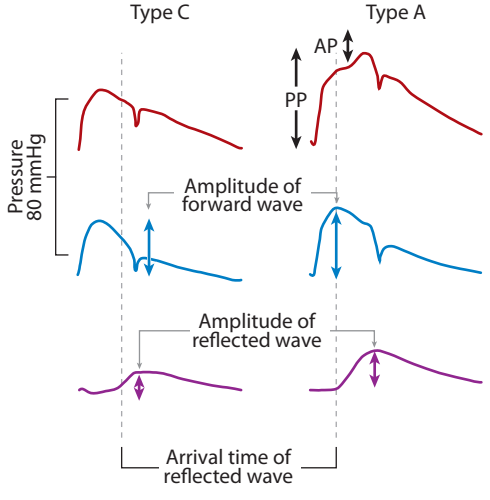

Figure 12

The aortic pressure waves in a young (type C) and older (type A) subject and the corresponding forward and backward components. A pronounced late systolic peak is marked AP and the pulse pressure is marked PP. Figure taken with permission from Westerhof et al. (2005).

waves measured in a young healthy adult (type C) and in an older subject (type A) as well as their corresponding forward and backward running components (Westerhof et al. 2005). In the young adult, the amplitude of the reflected wave is rather small and arrives relatively late in systole. The reflected wave peak takes place in early diastole; thus when added to the forward wave it does not create a significant increase in systolic pressure. In contrast, in the elderly subject, the reflected wave has larger amplitude and arrives early in systole. The addition of the reflected wave to the forward wave leads to a pronounced late systolic peak (marked AP in the figure), resulting in a considerable increase in systolic pressure. The late systolic peak in the type A subject is usually quantified by means of the augmentation index, defined as the ratio AP/PP, where the pulse pressure (PP) is defined as the difference between the peak systolic and the minimum diastolic pressure. The augmentation index has been a popular index in clinical studies relating systolic hypertension to arterial properties (stiffening) and to physiological (i.e., aging) or pathological (i.e., hypertension, arteriosclerosis) processes affecting wave speed and reflections.

3.4.2. Discrete transitions. If the length of a transition between two segments of the arterial tree is small compared to the wavelength, or even small compared to the radius, we talk about a discrete transition. The reflection phenomena at the transition then can be described on the basis of pressure and flow continuity across the transition. The incident pressure and flow waves represented by p_f and q_f are partly reflected and partly transmitted. The reflected waves can be denoted by p_b and q_b and the transmitted wave by p_t and q_t. Continuity of pressure and flow then yields

$$p_f + p_b = p_t \quad \text{and} \quad q_f + q_b = q_t. \tag{35}$$

The ratio between the complex amplitudes of the pressure and flow depends on the characteristic impedances Z_0 and Z_1 of the arterial segments connected:

$$\hat{p}_f = Z_0 \hat{q}_f, \quad \hat{p}_b = -Z_0 \hat{q}_b, \quad \text{and} \quad \hat{p}_t = Z_1 \hat{q}_t.$$

From this it follows that

$$Z_1 = \frac{\hat{p}_f + \hat{p}_b}{\hat{q}_f + \hat{q}_b}. \tag{36}$$

With the definition of the admittance $Y = 1/Z$ reflection and transmission coefficients, Γ and T can be defined according to

$$\Gamma = \frac{\hat{p}_b}{\hat{p}_f} = \frac{Y_0 - Y_1}{Y_0 + Y_1}, \quad T = \frac{\hat{p}_t}{\hat{p}_f} = \frac{2Y_0}{Y_1 + Y_0}. \tag{37}$$

So changes by geometrical discontinuities or in material properties that induce changes in the characteristic impedance will always lead to wave reflections defined by Equation 37.

3.4.3. Bifurcations. At bifurcations, continuity of pressure and conservation of mass yield

$$p_f + p_b = p_{t_1} + p_{t_2} \quad \text{and} \quad q_f + q_b = q_{t_1} + q_{t_2}. \tag{38}$$

Again using the characteristic admittances of the different branches, we obtain

$$\Gamma = \frac{Y_0 - (Y_1 + Y_2)}{Y_0 + (Y_1 + Y_2)}, \quad T_{12} = T_{21} = \frac{2Y_0}{Y_0 + (Y_1 + Y_2)}. \tag{39}$$

We note that, in bifurcations, conservation of mass does not imply continuity of flow. Consequently, in wave-propagation models of the arterial tree, bifurcation conditions can be implemented either as connecting interface conditions for the three parts or as an extra constraint that

enforces mass conservation (Bessems 2007). In the first case, methods of characteristics are needed to distinguish incoming from outgoing waves (Formaggia et al. 2003, Sherwin et al. 2003).

3.5. Boundary Conditions

In addition to geometrical and matrial transitions, in- and outflow conditions also can be responsible for wanted or unwanted wave reflections and therefore must be defined carefully. The most common possibilities are discussed in this section.

3.5.1. Lumped models as an outflow condition. At the entrance of an arterial network, a flow pulse as measured in reality, obtained from other models (see the next section), or based on theoretical considerations can be prescribed. At the outflow tracts, usually a terminal impedance representing the distal network of each truncated artery is prescribed. This terminal impedance can be modeled using a three-element windkessel model (Stergiopulos et al. 1992, Westerhof et al. 2009), consisting of a resistance R_c in series with a parallel combination of a capacitor C_t and another resistance R_p. In that case, the pressure and flow at the truncated arteries are related according to

$$\frac{\partial q}{\partial t} = \frac{1}{R_c}\frac{\partial p}{\partial t} + \frac{p}{R_c R_p C_t} - \left(\frac{R_c}{R_p} + 1\right)\frac{q}{R_c C_t}. \tag{40}$$

To obtain a good approximation of the parameters, one can follow different approaches (Mulder et al. 2010, Reymond et al. 2009). For example, one can choose to minimize high-frequency reflections at the transition from the 1D to the 0D domain by letting the characteristic resistance of the terminal impedance R_c be equal to the characteristic impedance of the truncated artery

$$R_c = Z_0 = \sqrt{\frac{L}{C}}. \tag{41}$$

The total peripheral resistance $R_t = R_c + R_p$ of each truncated artery can be derived from the total resistance R_T of the human arterial system in normal conditions. First, the resistance for each major part of the arterial network (i.e., head, upper or lower limbs) R_{BP} is determined by

$$R_{BP} = \frac{1}{\alpha_{BP}} R_T, \tag{42}$$

where a_{BP} is the realistic fraction of the cardiac output entering each body part. Second, within a body part compromising N_{BP} truncated arteries, it is assumed that the outflow of each truncated artery is proportional to its respective initial radius cubed (a_0^3) based on Murray's (1926) law or equivalently to an optimized value of the wall shear stress. The total resistance is then defined as

$$R_t = R_{BP}\frac{a_t^3}{a_0^3} \quad \text{with} \quad a_t^3 = \sum_{i=1}^{N_{BP}} a_{0,i}^3. \tag{43}$$

Finally, the terminal compliance C_t for each truncated artery can be assumed to be proportional to the flow fraction, R_T/R_t. Given that the sum of the compliances of the 1D segments and all 0D windkessel models equals the total compliance of the human body (i.e., $C_T = C_{1D} + C_{0D}$), the terminal compliance is defined as

$$C_t = C_{0D}\frac{R_T}{R_t}. \tag{44}$$

3.5.2. The heart as an inflow condition. At its proximal end (root of the ascending aorta), the arterial tree is coupled to the left ventricle of the heart. Despite the assumption of a prescribed flow, it is also possible to use a model of the heart (i.e., the ventricular contraction) and connect it to wave-propagation models of the arterial tree. This allows also the study of the interaction between heart mechanics and hemodynamics.

Time-varying elastance models. The left ventricular model suggested by Sagawa et al. (1988) is based on the time-varying elastance $E(t)$ concept of the left ventricle, which describes the variation of left ventricular pressure p_{lv} and volume V_{lv} during a cardiac cycle:

$$E(t) = \frac{p_{lv}(t)}{V_{lv}(t) - V_0}, \tag{45}$$

where V_0 is the dead volume of the left ventricle (**Figure 2**). The right lower panel of **Figure 2** shows the normalized varying elastance curve for one heart cycle. According to Senzaki et al. (1996), the normalized varying elastance curve is relatively invariable in young and old subjects and is relatively unaffected by various forms of disease. Hence, the varying elastance curve for any individual is fully determined by only three cardiac parameters, i.e., the maximal elastance E_{max}, the minimal elastance E_{min}, and the time to maximum elastance t_{max}. The empirical function $E(t)$ can be found in Senzaki et al. (1996).

Single-fiber models. An alternative to the varying elastance model is the use of one-fiber models of the heart, as introduced by Arts et al. (1991) and successfully extended and used by others (Bovendeerd et al. 2006, Cox et al. 2009) to model ventricular contraction as a function of pre- and afterload. The essential principle of this method is that for a spherical or cylindrical thick-walled cavity in which a contracting fiber is isotropically contracting, the ventricular volume V_{lv} is dependent on the fiber stretch λ_f according to

$$\lambda_f = \left(\frac{V_{lv} + \frac{1}{3} V_w}{V_0 + \frac{1}{3} V_w} \right)^{\frac{1}{3}}. \tag{46}$$

The pressure p_{lv} can be related to the fiber stress σ_f, left ventricular volume V_{lv}, and wall volume V_w according to

$$p_{lv} = \frac{1}{3} \sigma_f \ln \left(1 + \frac{V_w}{V_{lv}} \right). \tag{47}$$

The fiber stress σ_f is related to the fiber stretch λ_f according to a phenomenologically defined time-dependent relation:

$$\sigma_f = \sigma_f(\lambda_f, \dot{\lambda}_f, t). \tag{48}$$

The connection between the contraction models and the wave-propagation model of the arterial tree is mathematically straightforward. During ejection, however, the aortic valve, mostly modeled by a flow-dependent resistance, is open, and thus waves traveling backward in the aorta will be reflected according to the impedance mismatch between the proximal aorta and the left ventricle. During diastole, the valve is closed, and a complete reflection of the back traveling waves will occur. This is physiologically incorrect, and further refinements in the modeling of the valves with respect to wave reflections are needed.

3.5.3. The venous system to complete the circulation. Inflow boundary conditions for the arterial tree can be provided by simplified models of the heart, as indicated in the previous section. This, however, creates a new challenge to make a closed system that includes the veins. If one is

interested in arterial flow, the most obvious and straightforward way to include the venous system is to use a 0D model that at least contains the venous capacitive function. If, however, one is interested in detailed phenomena, two major aspects should be taken into account (Chow & Mak 2006). First, due to the low venous pressure p_v and the relatively high compliance of the veins, the local flow phenomena become more influential [$\rho v^2 = O(p_v)$] and also gravity forces become important. As a result, cross-sectional areas are not circular anymore, pressure-diameter relations are highly nonlinear, and a tendency to (or actual) collapse may occur. A second complicating factor is related to the presence of valves in the venous system. Pressure-flow relations become highly nonlinear, and the hemodynamic influence of valves cannot be easily integrated into the 1D formulation.

4. PHYSIOLOGICAL AND PATHOLOGICAL APPLICATIONS

4.1. Systemic Circulation

1D models have been used to study different aspects of wave phenomena in the arterial tree. The models vary substantially in their completeness (entire arterial tree or parts thereof); the nature of the model (lumped parameter, distributed or based on the 1D form of the Navier-Stokes equations); their treatment of nonlinearities, viscoelasticity, frictional terms, and bifurcations; and the choice or formulation of proximal (heart, input flow waveform) and distal (peripheral beds) boundary conditions.

A recurrent question in many 1D models concerns the accuracy of model predictions and the physiological relevance of results. Validation of 1D models has been performed at two levels: first at a purely qualitative level, by comparing model predictions of a typical or standard arterial tree with published pressure and flow waves at different arterial locations (see, e.g., Avolio 1980) or input impedance patterns in the aorta (e.g., Westerhof et al. 1969), and second at a semiquantitative level, by comparing model predictions with measurements performed on a specific subject or a group of subjects. Measurements typically involved flow measurements with Doppler ultrasound (e.g., Stettler et al. 1981) or magnetic resonance imaging (MRI) (e.g., Olufsen et al. 2000) and pressure measurements with tonometry (e.g., Reymond et al. 2009). Most authors conclude that 1D model predictions compare well with literature data and in vivo measurements. **Figure 13** shows such semiquantitative validation of the 1D model for systemic arteries, with a good agreement in wave shapes and in features between model predictions and measurements.

The in vivo validation of 1D models is difficult. The difficulty arises from the fact that a fully quantitative validation would require a subject-specific approach, in which all parameters defining the 1D model (geometry, viscoelastic properties, peripheral impedances, varying elastance of the heart) are measured or estimated precisely on a specific subject. Quantitative validations of the 1D model can be done, however, in vitro, either in single tubes (Bessems et al. 2008) or in networks of tubes resembling the arterial tree in geometry and elastic properties (Matthys et al. 2007). Bessems et al. (2008) studied wave propagation in a single tapered tube and showed good agreement between measured and predicted waves under the condition that viscoelastic wall properties are accounted for correctly.

4.2. Cerebral Circulation

Pressure and flow waves are not easily measured in deep cranial vessels of the cerebral circulation, such as the vessels in the vicinity of the circle of Willis. Hence, a number of groups resorted to the development of 1D models for predicting pressure and flow in the cerebral circulation (Alastruey et al. 2007; Hillen et al. 1982, 1986; Kufahl & Clark 1985; Papapanayotou et al. 1990;

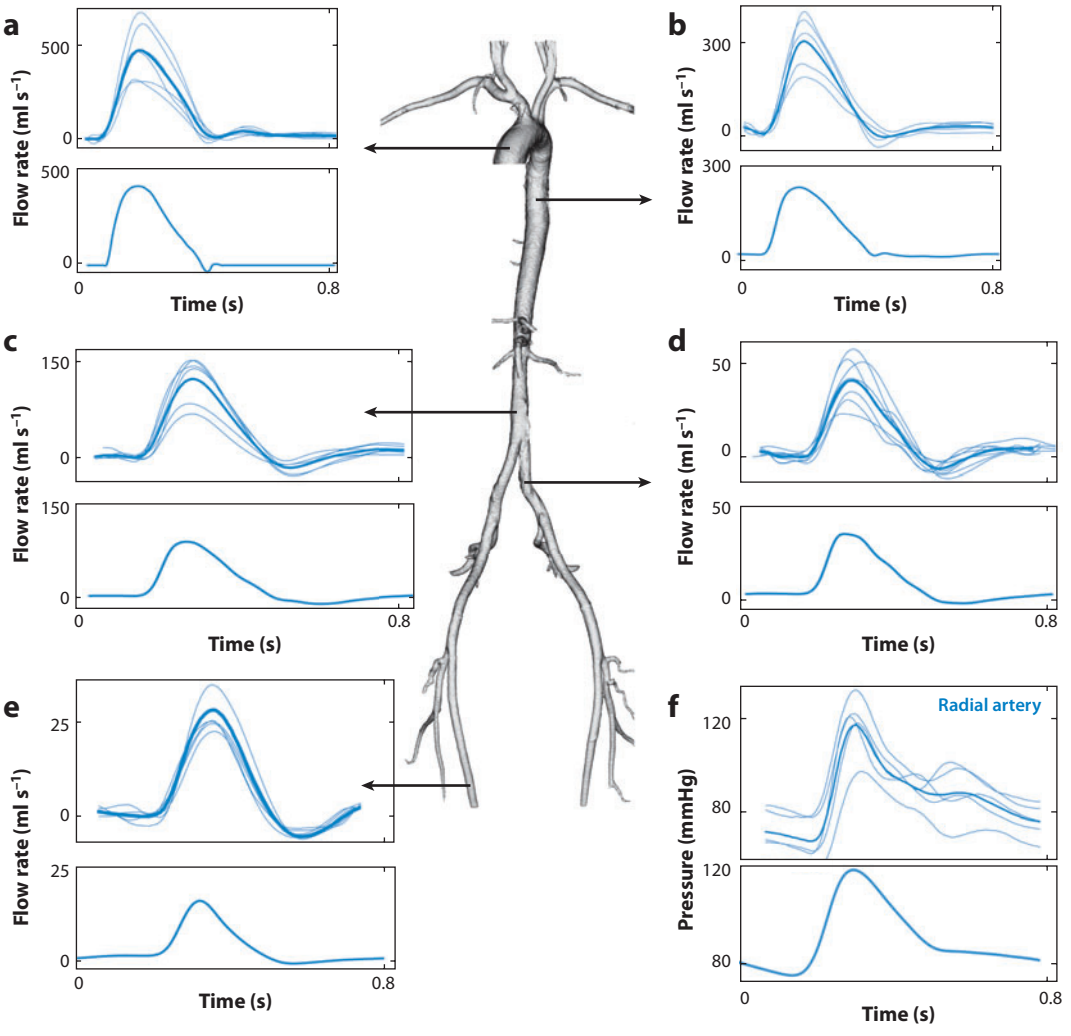

Figure 13

Semiquantitative comparison of 1D model predictions (*bottom of each panel*) and measurements of pressure and flow waves (*top of each panel*) at various systemic artery locations in a group of healthy young adults: (*a*) ascending aorta, (*b*) thoracic aorta, (*c*) abdominal aorta, (*d*) common iliac, (*e*) femoral artery, and (*f*) radial artery. Thick lines represent the averaged measured waveform at each arterial location. Figure taken with permission from Reymond et al. (2009).

Reymond et al. 2009; Zagzoule & Marc-Vergnes 1986). Models are often used to study the effects of stenoses (Kufahl & Clark 1985), vessel occlusions (Alastruey et al. 2007, Cassot et al. 2000), anatomical variations (Alastruey et al. 2007), and cerebral autoregulation (Alastruey et al. 2007, Zagzoule & Marc-Vergnes 1986). 1D models are also used to provide realistic boundary conditions for 3D CFD simulations in cerebral aneurysms (Ho et al. 2009). Validation of 1D model predictions of pressure and flow in the cerebral circulation was carried out by Reymond et al. (2009). Flow was measured by cranial ultrasound and pressure by applanation tonometry. **Figure 14** shows a comparison between measured and predicted waves. Waveform characteristics are well captured by the 1D model, thus validating the applicability of the model in the complex

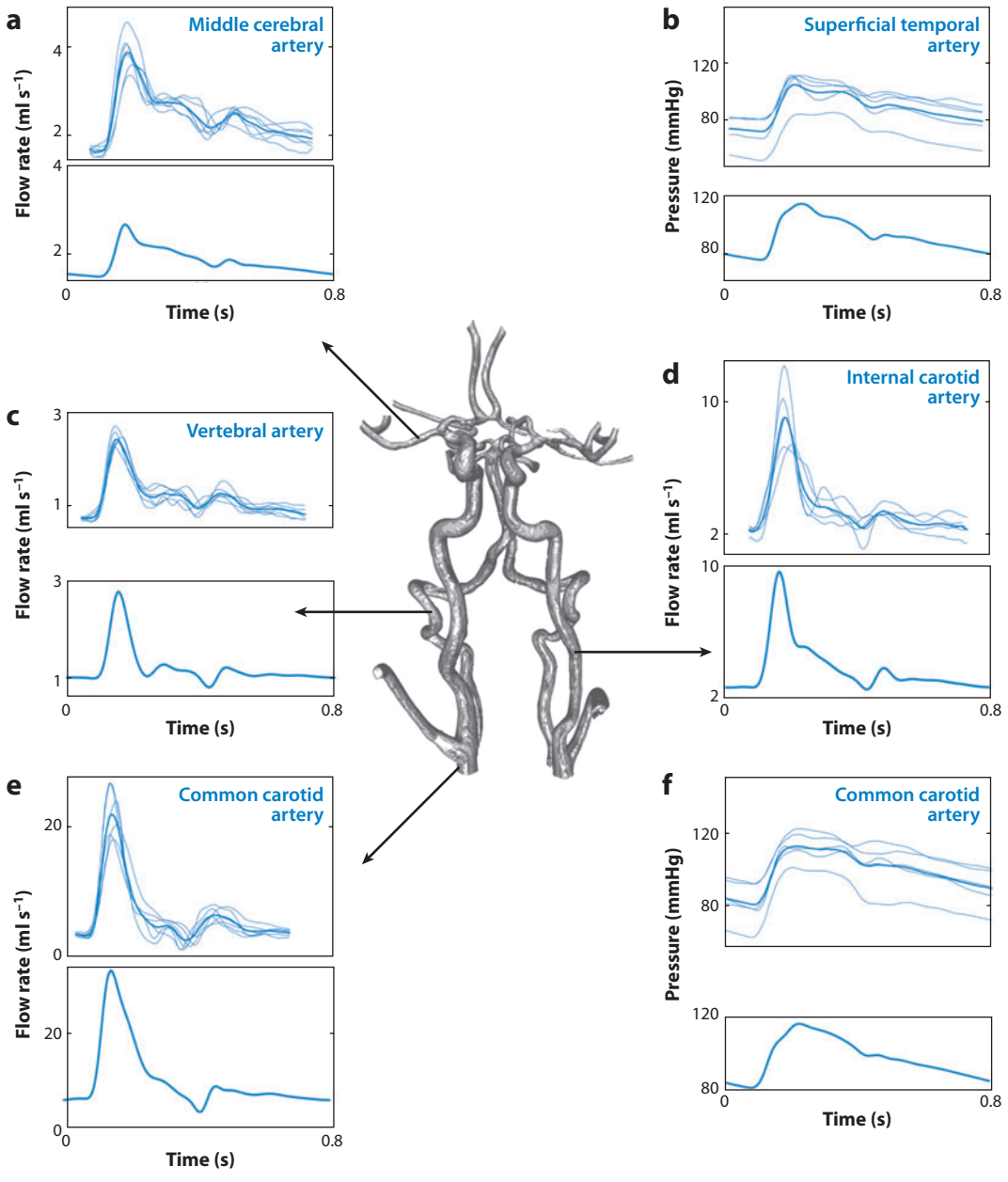

Figure 14

Semiquantitative comparison of 1D model predictions (*bottom of each panel*) and measurements of pressure and flow waves (*top of each panel*) at various cerebral artery locations in a group of healthy young adults. Thick lines represent the averaged measured waveform at each arterial location. Blood flow was measured with color-coded duplex ultrasound. Pressure was measured with applanation tonometry. Figure taken with permission from Reymond et al. (2009).

cerebral vascular system. Reymond et al. (2009) also showed that wave-reflection characteristics in the proximal cerebral vessels are correctly represented in the 1D model only in the presence of a detailed cerebral arterial tree, i.e., including the circle of Willis and all distal vasculature.

4.3. Coronary Circulation

Wave-propagation phenomena in the coronaries are more complex because of the effects of cardiac contraction on distal coronary beds. From a modeling standpoint, this requires an appropriate set of distal boundary conditions at terminal sites, which will account for the effect of myocardial contraction on peripheral resistances and compliances. This issue is addressed, to some extent, by the waterfall model (Downey & Kirk 1975) and the intramyocardial pump model (Arts & Reneman 1985). Bovendeerd et al. (2006) provided an improved description of the intramyocardial pressure by adding the effect of radial stress. In another, more phenomenological approach, Reymond et al. (2009) assumed that the distensibility and terminal coronary windkessel resistance and compliance changes during the heart cycle are proportional to the local varying elastance (Vis et al. 1995), which is assumed to be proportional to the varying elastance of the left ventricle.

Because of the short length of the coronaries in comparison to the wavelength and the presence of strong reflections throughout the cardiac cycle, estimation of wave speed based on two-point techniques or pressure-flow loops is not feasible. Davies et al. (2006) proposed a single-point technique, based on wave intensity analysis (Parker 2009b), although its accuracy has been questioned in subsequent clinical studies (Kolyva et al. 2008).

4.4. Stenoses and Aneurysms

Typical pathologies in the arterial system that have their influence on wave propagation phenomena are stenoses and aneurysms. A few remarks concerning these geometrical transitions in the arterial system are given below.

4.4.1. Stenoses. Stenoses are local narrowings in blood vessels, usually caused by the development of atheromatous plaques in the subintimal layer of the arterial wall. Stenoses cause significant pressure losses and can compromise the adequate perfusion of the distal vascular beds. Pressure losses over a stenosis can be treated through semiempirical relations, such as the one proposed by Young & Tsai (1973a,b):

$$\Delta p = \frac{8\pi\eta l}{A_s^2} q + \frac{K_t \rho}{2A_0^2}[A_0/A_s - 1]^2 q^2, \tag{49}$$

where A_0 is the unobstructed cross-sectional lumen area, and A_s is the minimal free cross-sectional lumen area within the coarctation. The first term accounts for the viscous losses (Poiseuille's law) as blood flows through the narrow coarctation lumen. The second term accounts for the pressure losses distal to the stenosis and is derived from the mechanics of flow in a tube with an abrupt expansion. K_t is an empirical coefficient approximately equal to 1.5, but strongly dependent on the shape of the stenosis. Extensions to unsteady flow can be found in Bessems (2007).

Stenoses affect wave-propagation characteristics. Incident waves passing through a stenosis get severely damped (Gosling et al. 1971, Stergiopulos et al. 1992). Stenoses also constitute an important wave-reflection site. Wave reflection and transmission properties of arterial stenoses have been analyzed using a quasi-nonlinear method by Stergiopulos et al. (1996). The results showed a strong dependence of the reflection coefficient modulus on stenosis severity, expressed as the ratio of the amplitude of the reflected wave to the amplitude of the incident wave.

4.4.2. Aneurysms. Abdominal aortic aneurisms (AAAs) are pathological dilations of the aorta, usually in the infrarenal area. AAAs may rupture, leading to severe hemorrhage and death. Therefore, close attention is focused on the aneurysm wall properties and the local stress and strain field, those being the principal biomechanical quantities affecting rupture risk. Studies have also focused on local flow characteristics because intimal shear is an important biomechanical cue driving aneurismal growth. AAAs constitute a major wave-reflection site, however, because of the substantial increase in arterial diameter and the changes in wall properties within an aneurysm. Swillens et al. (2008) studied the effect of AAAs on wave propagation in the aorta both experimentally and using a 1D model. Wave analysis showed that, in presence of an AAA, the reflection coefficient was negative as opposed to positive in the absence of an AAA. The negative reflection is attributed to a drop in characteristic impedance ($Z_c = \sqrt{\rho/AC}$) within the aneurysm. As both luminal area and local area compliance are inversely related to characteristic impedance, an AAA with larger luminal areas and more compliant walls would generate more negative reflections. An example of the application of a distributed model can be found in Wolters et al. (2007), who studied the aneurysmal pressure after endovascular repair of an aneurysm.

4.5. General Utility of 1D Models as Research and Clinical Tools

The examples presented above refer to the application of 1D models to the study of wave propagation in physiology and specific forms of arterial disease. 1D models have the capacity to be used as versatile research tools for simulating a variety of physiological and pathological phenomena and can be used for clinical decision-making support and surgical planning. A few examples of this large spectrum of 1D model applications are given below.

4.5.1. Model validation, parameter estimation, and inverse problems. The 1D models or distributed models of the entire circulation are used as virtual in vivo experimental setups, where all arterial parameters can be known and controlled independently. This offers the possibility of performing virtual experiments for assessing the validity of models or the accuracy of parameter-estimation techniques. For example, Stergiopulos et al. (1998) used a 1D model of the entire circulation to analyze the virtues and drawbacks of various forms of the windkessel models and derive what is claimed to be the most appropriate and precise four-element windkessel model of the systemic circulation (Stergiopulos et al. 1999). The same 1D model was used earlier to assess the accuracy of different methods for estimating total arterial compliance (Stergiopulos et al. 1995). 1D models can also be used to fit measured hemodynamical data and thus estimate different arterial parameters of interest. Such an approach was followed by Xiao et al. (2002) and Leguy et al. (2010), who used a distributed model and a 1D wave-propagation model of the human cardiovascular system to derive a parameter-estimation method that yields the best fit between measured and computed pressure and flow data.

4.5.2. Assessment of transfer function. Aortic pressure is a better indicator of cardiac morbidity and mortality than peripheral pressure. However, only peripheral pressures can be measured noninvasively. One way to obtain aortic pressure from measured peripheral pressure wave is to apply a so-called pressure to the transfer function. Transfer function, $H_p(\omega)$, defined in the frequency domain, is the ratio of the peripheral pressure wave, p_p, to the aortic pressure wave, p_{ao}. 1D models have been used to analyze the relationship between central aortic pressure and peripheral pressure in the arm (Karamanoglu et al. 1993), derive the main physical parameters defining the transfer function (Stergiopulos et al. 1998), and perform a sensitivity analysis on major determinants of transfer function (Westerhof et al. 2007).

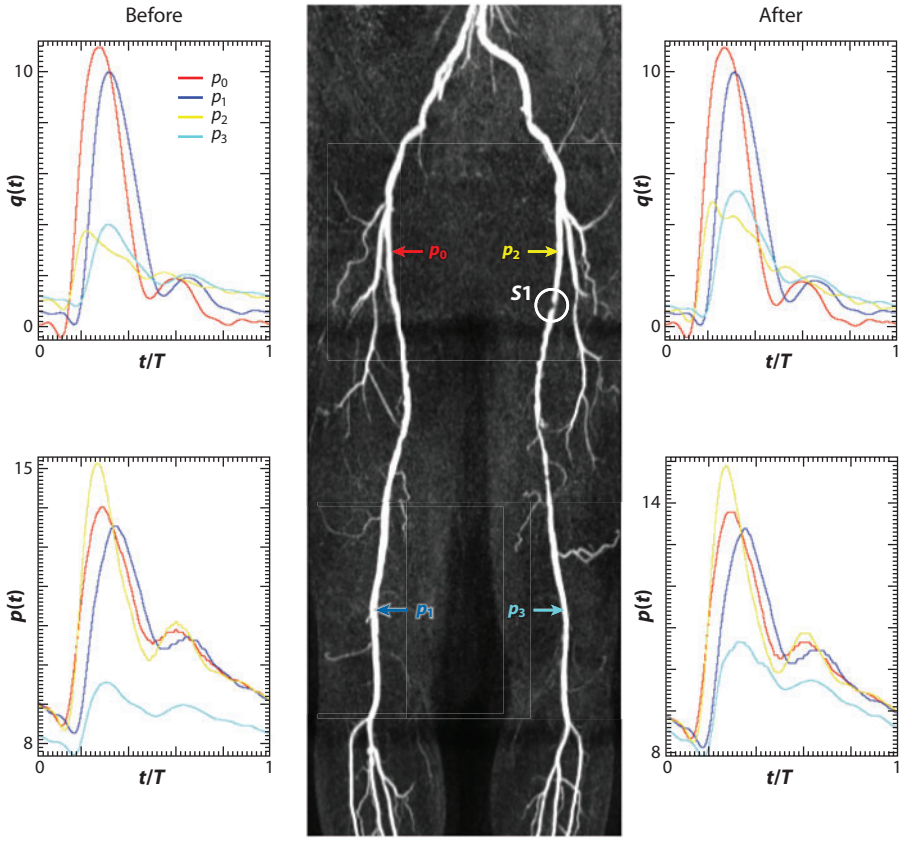

Figure 15

Flow and pressure before and after a partial reperfusion of the leg by means of angioplasty as determined by 1D wave-propagation modeling. Figure taken with permission from Bessems (2007).

4.5.3. Surgical planning. 1D models have been used to simulate the outcome of planned surgical procedures and thus provide insight for the best surgical approach (Taylor et al. 1999). Bessems (2007) reported predictions of the possible outcome of angioplasic reperfusion and bypass surgery in the leg based on a 1D wave-propagation model and MRI data (see **Figure 15**). A thorough clinical validation of this procedure is needed to define the predictive value of the model. Some first steps in the direction of such a validation have been made by Huberts et al. (2009a), who used the same model to predict the outcome of an arteriovenous fistula creation made for vascular access for dialysis patients, and encouraging results were obtained.

5. DISCUSSION AND CONCLUSIONS

5.1. Summary and Future Directions

The pulsatile nature of blood flow dictates numerous aspects of circulatory physiology and pathology. Pulsatility is manifested in pressure and flow waves propagating throughout the whole circulatory tree. Understanding the physical mechanisms of arterial wave propagation has been the objective of hemodynamicists for centuries. Waves result from the interaction of the heart with

the arterial system and thus carry significant diagnostic value, often unexploited to its fullest possible degree. In traditional clinical practice, only gross features of the pressure pulse, such as systolic and diastolic pressure, are used for diagnosis, prevention, and treatment. In recent years, more attention has been given to other wave characteristics and finer details of the pulse, such as the augmentation index, pulsatility index, and pulse pressure. As our techniques for noninvasive measurement of flow and pressure improve, we foresee an increase in the use of wave (intensity) analysis techniques (see Parker 2009b for a review) and wave-based information as part of future clinical practice. 1D models have been proven to be the most appropriate tools for analyzing wave-propagation phenomena in arteries. As seen in the present review, 1D models yield accurate predictions of pressure and flow, provided that model parameters faithfully represent the true physical quantities. Future developments in 1D models and their applications are likely to include the following.

5.1.1. Patient-specific modeling approaches. Model parameters are chosen to best fit a specific patient. A number of parameters can be measured with imaging techniques (i.e., geometry of arterial tree), whereas others can be obtained via noninvasive measurement techniques (e.g., Doppler, MRI, and tonometry). This approach is data intensive and can only be applied for research purposes at present.

5.1.2. Inverse modeling approaches and sensitivity analysis. One can combine 1D or lumped parameter models with experimental measurements as to best fit models to measured data and thus extract information on other quantities of interest for which direct measurements are not feasible. This should be combined with Monte Carlo–type sensitivity analyses to determine the critical parameters of the model, the required accuracy of the input data and boundary conditions, and the accuracy of the final model predictions.

5.1.3. Combination of 1D and 3D models. This approach has been already followed by many researchers and is likely to continue to be developed further. 1D models can be used to provide appropriate local boundary conditions to detailed 3D models at a specific arterial location.

5.1.4. Coupling with the venous and cerebrospinal fluid system. This is still an area of ongoing research, and few studies have dealt with the subjects so far. Coupling with the venous and CSF system requires appropriate modeling of the microcirculation and taking into account the particularities of venous and cerebospinal flow (e.g., valves and collapsible tubes). An effort in this direction is needed, however, to close the loop and provide a global model of the entire circulation.

5.1.5. Short-term adaptation mechanisms. To reflect the dynamic nature of the arterial tree, we should consider two important types of short-term adaptation mechanisms. First, in autoregulation, the microcirculation modeled with a linear windkessel model does not reflect the physiological behavior in vivo. Depending on the metabolic needs or local mechanical environment changes, short-term adaptation of the arterioles can significantly increase or decrease the peripheral resistance of one or more of the tissues that are perfused (Alastruey et al. 2008). Even more complicated models need to be developed to incorporate neurovascular coupling (Martens et al. 2009). Second, in flow-induced dilatation, when flow increases, local vascular smooth muscle tone decreases as a result of endothelium-dependent vasorelaxation mechanisms. Hence, even larger vessels may exhibit short-term adaptation to flow with small effects on resistance but likely larger consequences in compliance, suggesting that these type of effects should be included in the 1D

modeling. Flow-induced or mediated dilatation is of importance in the modeling of vascular access for hemodialysis (Huberts et al. 2009a).

5.1.6. Growth and remodeling. Growth and remodeling are processes that allow the living tissue to maintain an optimal environment and function under physiological development, aging, and disease. When exposed to sustained changes in flow or pressure, the arterial wall will respond by changing its geometry, structure (e.g., elastin and collagen content and architecture), and function. Hypertension leads to thickening of the arterial wall (hypertrophy), and it seems that wall thickening aims to restore hoop stress to control (normotensive) levels. Chronic changes in flow resulting in changes in wall shear stress lead to changes in arterial diameter that aim to restore intimal shear to control levels. Remodeling in response to increased flow is mediated by the endothelium and is associated with cell hyperplasia and structural changes in internal elastic lamina and adventitia. Remodeling leads to changes in compliance and resistance, affecting wave propagation and reflection characteristics of the arterial tree.

5.2. Conclusions

Wave propagation is an important aspect of arterial blood flow. Understanding wave phenomena and disposing the proper tools for analyzing pressure and flow waves can help researchers and clinicians obtain a deeper insight into the functioning of the cardiovascular system and eventually develop better diagnostic tools and possibly better therapies. Above we review the different approaches used for wave-propagation modeling and discuss their applications, their virtues, and drawbacks. We provide a detailed mathematical and physical background for the 1D models of the arterial circulation, which, in our opinion, are best suited for studying wave-propagation phenomena in the arterial tree. We foresee an increasing interest in the use of such 1D models, either as research tools or as support and decision-making tools in clinical practice.

DISCLOSURE STATEMENT

The authors are not aware of any affiliations, memberships, funding, or financial holdings that might be perceived as affecting the objectivity of this review.

LITERATURE CITED

Alastruey J, Moore SM, Parker KH, David T, Peiró J, Sherwin SJ. 2008. Reduced modelling of blood flow in the cerebral circulation: coupling 1-D, 0-D and cerebral auto-regulation models. *Int. J. Numer. Methods Fluids* 56:1061–67

Alastruey J, Parker KH, Peiro J, Byrd SM, Sherwin SJ. 2007. Modelling the circle of Willis to assess the effects of anatomical variations and occlusions on cerebral flows. *J. Biomech.* 40:1794–805

Anliker M, Rockwell RL, Ogden E. 1971. Non-linear analysis of flow pulses and shock waves in arteries, part I: derivation and properties of mathematical model. *Z. Angew. Math. Phys.* 22:217–46

Arts T, Bovendeerd PHM, Prinzen FW, Reneman RS. 1991. Relation between left ventricular cavity pressure and volume and systolic fiber stress and strain in the wall. *Biophys. J.* 59:93–102

Arts T, Reneman RS. 1985. Interaction between intramyocardial pressure (IMP) and myocardial circulation. *J. Biomech. Eng.* 107:51–56

Avolio A. 1980. Multi-branched model of the human arterial system. *Med. Biol. Eng. Comput.* 18:709–18

Azer K, Peskin CS. 2007. A one-dimensional model of blood flow in arteries with friction and convection based on the Womersley velocity profile. *Cardiovasc. Eng.* 7:51–73

Bessems D. 2007. *On the propagation of pressure and flow waves through the patient specific arterial system*. PhD thesis. Eindhoven Univ. Technol.

Bessems D, Giannopapa CG, Rutten MC, van de Vosse FN. 2008. Experimental validation of a time-domain-based wave propagation model of blood flow in viscoelastic vessels. *J. Biomech.* 41:284–91
Bessems D, Rutten MCM, van de Vosse FN. 2007. A wave propagation model of blood flow in large vessels using an approximate velocity profile function. *J. Fluid Mech.* 580:145–68
Beulen BWAMM, Rutten MCM, van de Vosse FN. 2009. A time-periodic approach for fluid-structure interaction in distensible vessels. *J. Fluids Struct.* 25:954–66
Boron WF, Boulpaep EL. 2003. *Medical Physiology*. Amsterdam: Elsevier
Bovendeerd PH, Borsje P, Arts T, van de Vosse FN. 2006. Dependence of intramyocardial pressure and coronary flow on ventricular loading and contractility: a model study. *Ann. Biomed. Eng.* 34:1833–45
Cassot F, Zagzoule M, Marc-Vergnes JP. 2000. Hemodynamic role of the circle of Willis in stenoses of internal carotid arteries: an analytical solution of a linear model. *J. Biomech.* 33:395–405
Chow KW, Mak CC. 2006. A simple model for the two dimensional blood flow in the collapse of veins. *J. Math. Biol.* 52:733–44
Cox LGE, Loerakker S, Rutten MCM, de Mol BAJM, van de Vosse FN. 2009. A mathematical model to evaluate control strategies for mechanical circulatory support. *Artif. Organs* 33:593–603
Damiano ER. 1998. The effect of the endothelial-cell glycocalyx on the motion of red blood cells through capillaries. *Microvasc. Res.* 55:77–91
Davies JE, Whinnett ZI, Francis DP, Willson K, Foale RA, et al. 2006. Use of simultaneous pressure and velocity measurements to estimate arterial wave speed at a single site in humans. *Am. J. Physiol. Heart Circ. Physiol.* 290:H878–85
Downey JM, Kirk ES. 1975. Inhibition of coronary blood flow by a vascular waterfall mechanism. *Circ. Res.* 36:753–60
Formaggia L, Lamponi D, Quarteroni A. 2003. One-dimensional models for blood flow in arteries. *J. Eng. Math.* 47:251–76
Frank O. 1899. Die grundform des arteriellen pulses. *Z. Biol.* 37:483–526
Gosling RG, Dunbar G, King DH, Newman DL, Side CD, et al. 1971. The quantitative analysis of occlusive peripheral arterial disease by a non-intrusive ultrasonic technique. *Angiology* 22:52–55
Guyton AC. 1967. *Textbook of Medical Physiology*. Philadelphia: Saunders
Harvey W. 1957 (1628). *Movement of the Heart and Blood in Animals*. Transl. K.J. Franklin. Oxford: Blackwell
Heil M, Hazel AL. 2011. Fluid-structure interaction in internal physiological flows. *Annu. Rev. Fluid Mech.* 43:141–62
Hillen B, Gaasbeek T, Hoogstraten HW. 1982. A mathematical model of the flow in the posterior communicating arteries. *J. Biomech.* 15:441–48
Hillen B, Hoogstraten HW, Post L. 1986. A mathematical model of the flow in the circle of Willis. *J. Biomech.* 19:187–94
Ho H, Sands G, Schmid H, Mithraratne K, Mallinson G, Hunter P. 2009. A hybrid 1D and 3D approach to hemodynamics modelling for a patient-specific cerebral vasculature and aneurysm. *Med. Image Comput. Comput. Assist. Interv.* 12:323–30
Holdsworth DW, Norley CJD, Fraynek R, Steinman DA, Rutt BK. 1999. Characterization of common carotid artery blood-flow waveforms in normal human subjects. *Physiol. Meas.* 20:219–40
Huberts W, Bosboom EMH, Planken RN, Tordoir JHM, van de Vosse FN. 2009a. Patient-specific computational modeling to improve the clinical outcome of vascular access creation. In *Vascular Access*, ed. JHM Tordoir, pp. 51–63. Turin: Ed. Minerva Med.
Huberts W, Bosboom EMH, van de Vosse FN. 2009b. A lumped model for blood flow and pressure in the systemic arteries based on an approximate velocity profile function. *Math. Biosci. Eng.* 6:27–40
Hughes TJR, Lubliner J. 1973. On the one-dimensional theory of blood flow in the large vessels. *Math. Biosci.* 18:161–70
Karamanoglu M, O'Rourke MF, Avolio AP, Kelly RP. 1993. An analysis of the relationship between central aortic and peripheral upper limb pressure waves in man. *Eur. Heart J.* 14:160–67
Kolyva C, Spaan JA, Piek JJ, Siebes M. 2008. Windkesselness of coronary arteries hampers assessment of human coronary wave speed by single-point technique. *Am. J. Physiol. Heart Circ. Physiol.* 295:H482–90
Kufahl RH, Clark ME. 1985. A circle of Willis simulation using distensible vessels and pulsatile flow. *J. Biomech. Eng.* 107:112–22

Leguy CAD, Bosboom EMH, Gelderblom H, Hoeks APG, van de Vosse FN. 2010. Estimation of distributed arterial mechanical properties using a wave propagation model in a reverse way. *Med. Eng. Phys.* In press

Lighthill J. 1978. *Waves in Fluids*. Cambridge, UK: Cambridge Univ. Press

Ling S, Atabek H. 1972. *J. Fluid Mech.* 55:493–511

Martens EGHJ, Peeters LLH, Gommer ED, Mess WH, van de Vosse FN, et al. 2009. The visually-evoked cerebral blood flow response in women with a recent history of preeclampsia and/or eclampsia. *Ultrasound Med. Biol.* 35:1–74

Matthys KS, Alastruey J, Peiro J, Khir AW, Segers P, et al. 2007. Pulse wave propagation in a model human arterial network: assessment of 1-D numerical simulations against in vitro measurements. *J. Biomech.* 40:3476–86

McDonald DA. 1974. *Blood Flow in Arteries*. London: Arnold. 2nd ed.

Mulder G, Bogaerds ACB, Rongen P, van de Vosse FN. 2010. The influence of contrast agent injection on physiological flow in the circle of Willis. *Med. Eng. Phys.* Manuscript submitted

Murray C. 1926. The physiological principle of minimum work. I. The vascular system and the cost of blood volume. *Physiology* 12:207–14

Olufsen M, Peskin C, Kim W, Pedersen E, Nadim A, Larsen J. 2000. Numerical simulation and experimental validation of blood flow in arteries with structured-tree outflow conditions. *Ann. Biomed. Eng.* 28:1281–99

Papapanayotou CJ, Cherruault Y, de la Rochefoucauld B. 1990. A mathematical model of the circle of Willis in the presence of an arteriovenous anomaly. *Comput. Math. Appl.* 20:199–206

Parker KH. 2009a. A brief history of arterial wave mechanics. *Med. Biol. Eng. Comput.* 47:111–18

Parker KH. 2009b. An introduction to wave intensity analysis. *Med. Biol. Eng. Comput.* 47:175–88

Patel DJ, Fry DL. 1966. Longitudinal tethering of arteries in dogs. *Circ. Res.* 14:1011–21

Pythoud F, Stergiopulos N, Bertram CD, Meister JJ. 1996. Effects of friction and nonlinearities on the separation of arterial waves into their forward and backward components. *J. Biomech.* 29:1419–23

Quarteroni A, Veneziani A. 2003. Analysis of a geometrical multiscale model based on the coupling of ODEs and PDEs for blood flow simulations. *Multiscale Model. Simul.* 1:173–95

Reymond P, Merenda F, Perren F, Rüfenacht D, Stergiopulos N. 2009. Validation of a one-dimensional model of the systemic arterial tree. *Am. J. Physiol. Heart Circ. Physiol.* 297:H208–22

Reynolds O. 1903. *Collected Work*, Vol. III: *Papers on Mechanical and Physical Subjects: The Sub-Mechanics of the Universe*. Cambridge, UK: Cambridge Univ. Press

Sagawa K, Maughan M, Suga H, Sunagawa K. 1988. *Cardiac Contraction and the Pressure-Volume Relationship*. New York: Oxford Univ. Press

Senzaki H, Chen CH, Kass DA. 1996. Valvular heart disease/heart failure/hypertension: single-beat estimation of end-systolic pressure-volume relation in humans: a new method with the potential for noninvasive application. *Circulation* 94:2497–506

Sherwin S, Franke V, Peirio J, Parker K. 2003. One-dimensional modelling of a vascular network in space-time variables. *J. Eng. Math.* 47:217–50

Stergiopulos N, Meister JJ, Westerhof N. 1995. Evaluation of methods for estimation of total arterial compliance. *Am. J. Physiol.* 268:H1540–48

Stergiopulos N, Spiridon M, Pythoud F, Meister JJ. 1996. On the wave transmission and reflection properties of stenoses. *J. Biomech.* 29:31–38

Stergiopulos N, Westerhof BE, Westerhof N. 1998. Physical basis of pressure transfer from periphery to aorta: a model-based study. *Am. J. Physiol.* 274:H1386–92

Stergiopulos N, Westerhof BE, Westerhof N. 1999. Total arterial inertance as the fourth element of the windkessel model. *Am. J. Physiol.* 276:H81–88

Stergiopulos N, Young DF, Rogge TR. 1992. Computer simulation of arterial flow with applications to arterial and aortic stenoses. *J. Biomech.* 25:1477–88

Stettler JC, Niederer P, Anliker M. 1981. Theoretical analysis of arterial hemodynamics including the influence of bifurcations. Part I: mathematical models and prediction of normal pulse patterns. *Ann. Biomed. Eng.* 9:145–64

Swillens A, Lanoye L, De Backer J, Stergiopulos N, Verdonck PR, et al. 2008. Effect of an abdominal aortic aneurysm on wave reflection in the aorta. *IEEE Trans. Biomed. Eng.* 55:1602–11

Taylor CA, Draney MT, Ku JP, Parker D, Steele BN, et al. 1999. Predictive medicine: computational techniques in therapeutic decision-making. *Comput. Aided Surg.* 4:231–47

Taylor CA, Figueroa CA. 2009. Patient-specific modeling of cardiovascular mechanics. *Annu. Rev. Biomed. Eng.* 11:109–34

van de Vosse FN, de Hart J, van Oijen CHGA, Bessems D, Gunther TWM, et al. 2003. Finite-element-based computational methods for cardiovascular fluid-structure interaction. *J. Eng. Math.* 47:335–68

Vis MA, Sipkema P, Westerhof N. 1995. Modeling pressure-area relations of coronary blood vessels embedded in cardiac muscle in diastole and systole. *Am. J. Physiol.* 268:H2531–43

Wan J, Steele B, Spicer SA, Strohband S, Feijoo GR, et al. 2002. A one-dimensional finite element method for simulation-based medical planning for cardiovascular disease. *Comput. Methods Biomech. Biomed. Eng.* 5:195–206

Westerhof BE, Guelen I, Stok WJ, Wesseling KH, Spaan JA, et al. 2007. Arterial pressure transfer characteristics: effects of travel time. *Am. J. Physiol. Heart Circ. Physiol.* 292:H800–7

Westerhof N, Bosman F, De Vries CJ, Noordergraaf A. 1969. Analog studies of the human systemic arterial tree. *J. Biomech.* 2:121–43

Westerhof N, Elzinga G, Sipkema P. 1971. An artificial arterial system for pumping hearts. *J. Appl. Physiol.* 31:776–81

Westerhof N, Lankhaar JW, Westerhof BE. 2009. The arterial windkessel. *Med. Biol. Eng. Comput.* 47:131–41

Westerhof N, Sipkema P, Van Den Bos GC, Elzinga G. 1972. Forward and backward waves in the arterial system. *Cardiovasc. Res.* 6:648–56

Westerhof N, Stergiopulos N, Noble MIM. 2005. *Snapshots of Hemodynamics: An Aid for Clinical Research and Graduate Education*. New York: Springer

Witzig S. 1914. *Über erzwungene wellenbewegungen zäher inkompressibler flüssigkeiten in elastischen rohren*. Inan. diss. Univ. Bern

Wolters BJBM, Emmera M, Rutten MCM, Schurink GWH, van de Vosse FN. 2007. Assessment of endoleak significance after endovascular repair of abdominal aortic aneurysms: a lumped parameter model. *Med. Eng. Phys.* 29:1106–18

Womersley JR. 1955. Mathematical theory of oscillating flow in an elastic tube. *J. Physiol.* 127:553–63

Womersley JR. 1957. An elastic tube theory of pulse transmission and oscillatory flow in mammalian arteries. *Tech. Rep. WADC-TR-56-614*, Wright Air Dev. Center, Dayton, OH

Xiao X, Ozawa ET, Huang Y, Kamm RD. 2002. Model-based assessment of cardiovascular health from noninvasive measurements. *Ann. Biomed. Eng.* 30:612–23

Young DF, Tsai FY. 1973a. Flow characteristics in models of arterial stenoses. I. Steady flow. *J. Biomech.* 6:395–410

Young DF, Tsai FY. 1973b. Flow characteristics in models of arterial stenoses. II. Unsteady flow. *J. Biomech.* 6:547–59

Young T. 1809. On the functions of the heart and arteries. *Philos. Trans.* 99:1–31

Zagzoule M, Marc-Vergnes JP. 1986. A global mathematical model of the cerebral circulation in man. *J. Biomech.* 19:1015–22